NATIONAL & KAPODISTRIAN
UNIVERSITY OF ATHENS
DEPARTMENT OF PHYSICS
SECTION OF CONDENSED MATTER PHYSICS

Geometric phase calculation in crystalline solids and applications in Hall effects

Theodoros Adamantopoulos
M.Sc. Thesis

Supervisor:
Phivos Mavropoulos
Professor

ATHENS 2020

ΕΘΝΙΚΟ & ΚΑΠΟΔΙΣΤΡΙΑΚΟ
ΠΑΝΕΠΙΣΤΗΜΙΟ ΑΘΗΝΩΝ
ΤΜΗΜΑ ΦΥΣΙΚΗΣ
ΤΟΜΕΑΣ ΦΥΣΙΚΗΣ ΣΥΜΠΥΚΝΩΜΕΝΗΣ ΥΛΗΣ

Υπολογισμός της γεωμετρικής φάσης σε κρυσταλλικά στερεά και εφαρμογές στα φαινόμενα Hall

Θεόδωρος Αδαμαντόπουλος

Διπλωματική Εργασία

Επιβλέπων:
Φοίβος Μαυρόπουλος
Καθηγητής

ΑΘΗΝΑ 2020

Acknowledgements

First of all, I would like to thank Prof. Phivos Mavropoulos for supervising this thesis and giving me the chance to study this very interesting topic. His guidance and constant support were very important for the accomplishment of this work. Also, very helpful was his willingness to provide explanations and discuss about physics.

I am thankful to Prof. Dimitrios Frantzeskakis and Prof. Konstantinos Sfetsos for their willingness to devote time assessing this thesis as committee members.

I am grateful to Adamantia Kosma for her help concerning the Jülich KKR code and other computational issues. Also, I would like to thank her for proofreading this thesis.

Last but not least, I would like to thank my family and my friends for their support throughout the years of my studies.

This work was supported by computational time granted from the Greek Research & Technology Network (GRNET) in the National HPC facility - ARIS - under project ID pr007039_thin-TopMagX.

Abstract

In the present master thesis a formalism is developed for obtaining the geometric phase and the Berry curvature, within the framework of the relativistic multiple scattering Korringa-Kohn-Rostoker (KKR) method and the density functional theory for the calculation of the electronic structure of solids. The physical significance of geometric phase is known to be featured, among others, to the anomalous Hall effect theory. The Berry curvature which is defined by the Bloch states over the energy bands, stems from the spin-orbit interaction and exhibits very strong variations in the points where the degeneracy of the energy bands due to this interaction is raised. The formalism is applied in the case of the ferromagnetic bcc Fe, for which the numerical stability of the method and the dependence on the spin-orbit interaction strength is examined in a series of numerical experiments. Finally, the temperature dependence of the anomalous Hall conductivity is also studied.

Περίληψη

Στην παρούσα διπλωματική εργασία αναπτύσσεται ο φορμαλισμός εύρεσης της γεωμετρικής φάσης (Berry phase) και της γεωμετρικής καμπυλότητας (Berry curvature) για σιδηρομαγνητικά υλικά, στο πλαίσιο της σχετικιστικής μεθόδου πολλαπλής σκέδασης των Korringa, Kohn και Rostoker (KKR) και της θεωρίας συναρτησιακού της πυκνότητας για τον υπολογισμό της ηλεκτρονικής δομής των στερεών. Η φυσική σημασία της γεωμετρικής φάσης είναι γνωστό ότι αναδεικνύεται, μεταξύ άλλων, στη θεωρία του ανώμαλου φαινομένου Hall. Η γεωμετρική καμπυλότητα, που ορίζεται μέσω των καταστάσεων Bloch πάνω στις ενεργειακές ζώνες, εκρέει από την αλληλεπίδραση σπιν-τροχιάς και παρουσιάζει πολύ ισχυρές διακυμάνσεις στα σημεία όπου αίρεται ο εκφυλισμός των ενεργειακών ζωνών λόγω αυτής της αλληλεπίδρασης. Ο φορμαλισμός εφαρμόζεται στην περίπτωση του σιδηρομαγνητικού bcc Fe, για την οποία εξετάζεται η αριθμητική ευστάθεια της μεθόδου και η εξάρτηση από την ισχύ της αλληλεπίδρασης σπιν-τροχιάς σε μια σειρά από αριθμητικά πειράματα. Τέλος, μελετάται και η εξάρτηση της ανώμαλης αγωγιμότητας Hall από την θερμοκρασία.

Contents

Chapter 1

Introduction

The concept of geometric phase was first introduced by M. Berry in 1984 [1]. He discovered that, when a system described by a parameter-dependent Hamiltonian evolves adiabatically around a closed path, it acquires a phase. Because that phase results from the geometrical properties of the parameter space, he named it geometric phase. However, it is more commonly established as Berry phase and, together with the Berry connection and the Berry curvature, they are the basis of the Berry phase theory. The Berry phase depends only on the geometry of the closed path and not on the parameter rate of change on it, as long as the adiabatic approximation holds. Also, the Berry phase is a gauge-invariant quantity.

Berry's discovery showed that the mathematical concepts of geometry and topology can enter in many fields of Condensed Matter Physics. This helped into better understanding, predicting and discovering various effects [2]. Some of them are the family of Hall effects in metals and insulators, the field of topological materials, the electric polarization and the orbital magnetization.

As far as the interest of this thesis is concerned, the Berry phase theory gave the opportunity to reformulate the semi-classical equations of motion and interpret the anomalous velocity in terms of the Berry curvature [3]. This led to attribute the intrinsic mechanism behind the anomalous Hall effect to the Berry curvature that is derived from the occupied Bloch states. The significance of this discovery was that it made possible to examine the charge and spin transport properties in solids via first-principles calculations.

In this thesis, the Berry curvature of Bloch states is calculated within the KKR framework, following the implementation of Gradhand et al. [4]. The studied system is the ferromagnetic bcc Fe. Compared to [4], the Dirac equation is solved within the full-potential scalar relativistic approximation, with the addition of a correction representing the SOC. Also, a different choice for the normalization of the scattering solutions is made. Consequently, a new set of equations is derived for the Abelian Berry connection and the Abelian Berry curvature. The equations are expressed in terms of the eigenvectors and the eigenvalues of the KKR matrix. The calculated Berry curvature is then

used to find the intrinsic anomalous Hall conductivity. It should be noted that the Berry phase method is complementary to the Kubo-Bastin formula that was implemented by Ködderitzsch et al. [5] in the relativistic KKR formalism within the Coherent Potential Approximation (CPA) that treats chemical disorder in an element-specific manner.

This thesis is structured as follows. In Chapter 2, the general concept of Berry phase is studied. At first it is introduced for an abstract quantum mechanical system and then it is applied on the Bloch electrons of a crystalline solid. Also, the fundamental expressions for the Berry phase, the Berry connection and the Berry curvature are presented.

In Chapter 3, the KKR Green function method is presented. Firstly, a brief definition of the Green function is given. Afterwards, the single-site scattering problem is examined and then, the multiple scattering problem from all the atoms within the crystal is solved. From the solution of the multiple scattering problem, follows the formulation of the KKR wavefunctions.

In Chapter 4, the anomalous Hall effect is reviewed. Starting from an introduction to its origins and a historical overview of its study, focus is given to the intrinsic mechanism behind it. The semi-classical equations of motion are reformulated by considering a wave-packet constructed from Bloch states, under the presence of external fields up to first order. In this way, an expression for the anomalous velocity is derived in terms of the Berry curvature. Last, for the electron transport problems, the intrinsic anomalous Hall conductivity can be calculated from the Berry curvature.

In Chapter 5, the method to calculate the Berry curvature within the KKR framework, developed for the purpose of this thesis, is described. The resulting equations for the Berry connection and the Berry curvature depend on the eigenvectors and the eigenvalues of the KKR matrix. The normalization of the KKR wavefunctions implies a special treatment for the calculation of the derivative of the eigenvectors. This treatment is also analyzed. Moreover, the KKR representation of matrices which appear in the relations for the Berry curvature is presented. The matrices contain an integration over the unit cell, which is also treated specially in the KKR framework, because of the entrance of the shape functions and the expansions in spherical harmonics. A method to calculate vector matrices with integrals of four spherical harmonics is developed. Finally, the relation to calculate the anomalous Hall conductivity from the energy resolved Berry curvature is introduced.

Chapter 6 contains the results of the calculations for the ferromagnetic bcc Fe. At first, the Berry curvature at the Fermi surface is studied. Then, the energy resolved Berry curvature is examined. In the end, the anomalous Hall conductivity is calculated. In the discussion of the results, the dependence of the Berry curvature on the spin-orbit coupling is understood. Furthermore, the behavior of the Berry curvature under the scaling of the spin-orbit coupling strength is seen and a comparison to other works is made.

Chapter 2

Berry phase in quantum mechanics

The basic aspects of the Berry phase concept introduced in the following Chapter are based on the Refs. [2] and [6].

2.1 Berry phase and adiabatic evolution

At first, a quantum system described by a Hamiltonian that depends on a parameter set $\boldsymbol{\lambda} = (\lambda_1, \lambda_2, ...)$ is considered. The Hamiltonian $\hat{\mathcal{H}}(\boldsymbol{\lambda})$ and its discrete eigenspectrum $\{\epsilon_n(\boldsymbol{\lambda})\}$ are assumed to be smooth (have continuous derivatives) and unique functions of $\boldsymbol{\lambda}$ in the parameter space. For the instantaneous set of eigenstates $\{|n\boldsymbol{\lambda}\rangle\}$ of this Hamiltonian holds

$$\hat{\mathcal{H}}(\boldsymbol{\lambda})|n\boldsymbol{\lambda}\rangle = \epsilon_n(\boldsymbol{\lambda})|n\boldsymbol{\lambda}\rangle. \tag{2.1}$$

The eigenstates $\{|n\boldsymbol{\lambda}\rangle\}$ are not completely determined from (2.1), as an arbitrary $\boldsymbol{\lambda}$-dependent phase factor of $\{|n\boldsymbol{\lambda}\rangle\}$ is still allowed. This arbitrariness can be removed if the following *gauge transformation* is made

$$|n\boldsymbol{\lambda}\rangle' = e^{i\zeta_n(\boldsymbol{\lambda})}|n\boldsymbol{\lambda}\rangle. \tag{2.2}$$

The arbitrary complex phase factor $\zeta_n(\boldsymbol{\lambda})$, also called *gauge*, is considered smooth and single valued along these regions of the parameter space. The freedom of choice between $\{|n\boldsymbol{\lambda}\rangle\}$ and $\{|n\boldsymbol{\lambda}\rangle\}'$ is called *gauge freedom*.

During the time evolution of the system, the parameter $\boldsymbol{\lambda}(t)$ is considered to move along a closed path $\mathcal{C}$ in the parameter space, with a period T such that $\boldsymbol{\lambda}(0) = \boldsymbol{\lambda}(T)$. The time-dependent Schrödinger equation of the system is

$$\hat{\mathcal{H}}(\boldsymbol{\lambda}(t))|\psi(t)\rangle = i\hbar\frac{\partial}{\partial t}|\psi(t)\rangle. \tag{2.3}$$

The system is considered to evolve according to the adiabatic approximation [7], which means that it remains in its instantaneous eigenstate throughout the time evolution. A

state $|\psi\rangle$ can be written as

$$|\psi(t)\rangle = e^{i\gamma_n(t)} e^{-i\alpha_{dyn}(t)} |n\boldsymbol{\lambda}(t)\rangle, \tag{2.4}$$

where $\alpha_{dyn}(t) = \frac{1}{\hbar}\int_0^t \epsilon_n(t')dt'$ is the *dynamical phase* obtained due to the time evolution. The first exponential term is the *geometric*, or more commonly known as *Berry phase*. By demanding that $|\psi(t)\rangle$ satisfies (2.3), γ_n is given by [1]

$$\gamma_n = i \oint_{\mathcal{C}} \langle n\boldsymbol{\lambda}|\nabla_{\boldsymbol{\lambda}}|n\boldsymbol{\lambda}\rangle d\boldsymbol{\lambda}. \tag{2.5}$$

Thus, the Berry phase depends only on the geometric properties of the closed path $\mathcal{C}$ and is independent of the way that $\boldsymbol{\lambda}(t)$ varies in time, as long as it is slow enough for the adiabatic approximation to hold. It is obtained due to the variation of the state with the changing Hamiltonian. It follows from the normalization $\langle n\boldsymbol{\lambda}|n\boldsymbol{\lambda}\rangle = 1$, that $\langle n\boldsymbol{\lambda}|\nabla_{\boldsymbol{\lambda}}|n\boldsymbol{\lambda}\rangle = -\langle n\boldsymbol{\lambda}|\nabla_{\boldsymbol{\lambda}}|n\boldsymbol{\lambda}\rangle^*$ for any $\boldsymbol{\lambda}$, so Berry phase is a purely real quantity.

In the gauge transformation considered in (2.2) the phase $e^{i\zeta_n(\boldsymbol{\lambda})}$ is single valued, since along the closed path $\mathcal{C}$

$$\zeta_n(\boldsymbol{\lambda}(0)) - \zeta_n(\boldsymbol{\lambda}(T)) = 2\pi \times integer. \tag{2.6}$$

So the gauge transformation (2.2) yields for γ_n

$$\gamma_n' = \gamma_n - \oint_{\mathcal{C}} d\zeta_n = \gamma_n. \tag{2.7}$$

This means that the Berry phase is a gauge-invariant quantity. The fact that M. Berry chose the parameter $\boldsymbol{\lambda}$ to move along a closed path $\mathcal{C}$ gave physical meaning to the geometric phase. For a simple, constant in time, parameter-dependent Hamiltonian, only the dynamical phase $\alpha_{dyn}(t)$ occurs after time evolution. If the Hamiltonian evolves in time according to the adiabatic approximation but the path $\mathcal{C}$ is not closed, then a geometric phase also occurs, but it can be canceled out by a suitable gauge choice. A more detailed analysis about the geometric phase can be found in [7].

2.2 Berry connection and Berry curvature

The expression for the Berry phase (2.5) can be written in the form

$$\gamma_n = \oint_{\mathcal{C}} \boldsymbol{\mathcal{A}}_n(\boldsymbol{\lambda}) d\boldsymbol{\lambda}, \tag{2.8}$$

where the *Berry connection* $\boldsymbol{\mathcal{A}}_n$ is introduced as the vector field

$$\boldsymbol{\mathcal{A}}_n(\boldsymbol{\lambda}) = i\langle n\boldsymbol{\lambda}|\nabla_{\boldsymbol{\lambda}}|n\boldsymbol{\lambda}\rangle. \tag{2.9}$$

It is obvious that the Berry connection is a purely real quantity. Although, unlike the Berry phase, it is not gauge-invariant and thus not observable. A gauge transformation (2.2) for the connection gives

$$\boldsymbol{\mathcal{A}}'_n = \boldsymbol{\mathcal{A}}_n - \nabla_{\boldsymbol{\lambda}}\zeta_n. \tag{2.10}$$

The *Berry curvature* $\boldsymbol{\Omega}_n$ is defined as an anti-symmetric, second-rank, field tensor with components

$$\Omega^n_{ij}(\boldsymbol{\lambda}) = \partial_{\lambda_i}\mathcal{A}^n_j(\boldsymbol{\lambda}) - \partial_{\lambda_j}\mathcal{A}^n_i(\boldsymbol{\lambda}) = -2\mathrm{Im}\left\langle \frac{\partial}{\partial_{\lambda_i}} n\boldsymbol{\lambda} \middle| \frac{\partial}{\partial_{\lambda_j}} n\boldsymbol{\lambda} \right\rangle. \tag{2.11}$$

By its definition, the Berry curvature is purely real and gauge-invariant under the gauge transformation (2.2), so it is also observable. If the parameter space is three-dimensional, with the help of Stoke's theorem, the Berry phase (2.5) can be written as

$$\gamma_n = \oint_{\mathcal{C}} \boldsymbol{\mathcal{A}}_n(\boldsymbol{\lambda}) d\boldsymbol{\lambda} = \int_{\mathcal{S}} \boldsymbol{\Omega_n}(\boldsymbol{\lambda}) d\mathbf{S}, \tag{2.12}$$

so Berry curvature can be seen in a pseudovector form as

$$\boldsymbol{\Omega}_n(\boldsymbol{\lambda}) = \nabla_{\boldsymbol{\lambda}} \times \boldsymbol{\mathcal{A}}_n(\boldsymbol{\lambda}). \tag{2.13}$$

The Berry curvature components are related to its tensor form via the relation

$$\boldsymbol{\Omega}^n_i = \frac{1}{2}\epsilon_{ijk}\Omega^n_{jk}, \tag{2.14}$$

with ϵ_{ijk} the Levi-Civita anti-symmetric tensor. In analogy to electrodynamics, $\boldsymbol{\Omega}_n$ can be seen as a vector field derived from the vector potential $\boldsymbol{\mathcal{A}}_n$ and γ_n as the flux of $\boldsymbol{\Omega}_n$ through $\mathcal{S}$.

A more computationally useful relation for the Berry curvature can be obtained, if it is expressed in terms of the eigenstates of the Hamiltonian. With the help of the completeness relation of the eigenstates set, the equation (2.13) can be written as

$$\boldsymbol{\Omega}_n(\boldsymbol{\lambda}) = -\mathrm{Im}\langle \nabla_{\boldsymbol{\lambda}} n\boldsymbol{\lambda}| \times |\nabla_{\boldsymbol{\lambda}} n\boldsymbol{\lambda}\rangle \tag{2.15}$$

$$= -\mathrm{Im}\sum_{m\neq n} \langle \nabla_{\boldsymbol{\lambda}} n\boldsymbol{\lambda}|m\boldsymbol{\lambda}\rangle \times \langle m\boldsymbol{\lambda}|\nabla_{\boldsymbol{\lambda}} n\boldsymbol{\lambda}\rangle. \tag{2.16}$$

Using the relation $\langle n\boldsymbol{\lambda}|m\boldsymbol{\lambda}\rangle = \delta_{nm}$ follows that $\langle n\boldsymbol{\lambda}|\nabla_{\boldsymbol{\lambda}} m\boldsymbol{\lambda}\rangle = -\langle \nabla_{\boldsymbol{\lambda}} n\boldsymbol{\lambda}|m\boldsymbol{\lambda}\rangle$. Then,

together with the fact that the Hamiltonian operator is Hermitian, (2.1) gives

$$\nabla_{\boldsymbol{\lambda}}\hat{\mathcal{H}}(\boldsymbol{\lambda})|n\boldsymbol{\lambda}\rangle + \hat{\mathcal{H}}(\boldsymbol{\lambda})|\nabla_{\boldsymbol{\lambda}} n\boldsymbol{\lambda}\rangle = \nabla_{\boldsymbol{\lambda}}\epsilon_n(\boldsymbol{\lambda})|n\boldsymbol{\lambda}\rangle + \epsilon_n(\boldsymbol{\lambda})|\nabla_{\boldsymbol{\lambda}} n\boldsymbol{\lambda}\rangle \tag{2.17}$$

$$\overset{\cdot\langle m\boldsymbol{\lambda}|}{\underset{m\neq n}{\Longrightarrow}} \langle m\boldsymbol{\lambda}|\nabla_{\boldsymbol{\lambda}}\hat{\mathcal{H}}(\boldsymbol{\lambda})|n\boldsymbol{\lambda}\rangle + \epsilon_m(\boldsymbol{\lambda})\langle m\boldsymbol{\lambda}|\nabla_{\boldsymbol{\lambda}} n\boldsymbol{\lambda}\rangle = \epsilon_n(\boldsymbol{\lambda})\langle m\boldsymbol{\lambda}|\nabla_{\boldsymbol{\lambda}} n\boldsymbol{\lambda}\rangle \tag{2.18}$$

$$\Longrightarrow \langle m\boldsymbol{\lambda}|\nabla_{\boldsymbol{\lambda}} n\boldsymbol{\lambda}\rangle = \frac{\langle m\boldsymbol{\lambda}|\nabla_{\boldsymbol{\lambda}}\hat{\mathcal{H}}(\boldsymbol{\lambda})|n\boldsymbol{\lambda}\rangle}{\epsilon_n(\boldsymbol{\lambda}) - \epsilon_m(\boldsymbol{\lambda})}, \quad \text{for} \quad m \neq n. \tag{2.19}$$

Therefore, for the Berry curvature yields

$$\boldsymbol{\Omega}_n(\boldsymbol{\lambda}) = -\mathrm{Im}\sum_{m\neq n} \frac{\langle n\boldsymbol{\lambda}|\nabla_{\boldsymbol{\lambda}}\hat{\mathcal{H}}(\boldsymbol{\lambda})|m\boldsymbol{\lambda}\rangle \times \langle m\boldsymbol{\lambda}|\nabla_{\boldsymbol{\lambda}}\hat{\mathcal{H}}(\boldsymbol{\lambda})|n\boldsymbol{\lambda}\rangle}{[\epsilon_n(\boldsymbol{\lambda}) - \epsilon_m(\boldsymbol{\lambda})]^2}. \tag{2.20}$$

The latter equation is very useful for numerical calculations because only the diagonalization of the Hamiltonian is needed and the differentiation of the eigenstates is avoided. The eigenvalue difference in the denominator denotes that when two eigenvalues are close the Berry curvature becomes larger and even diverges. This happens at degeneracy ($\epsilon_n = \epsilon_m$) and near degeneracy ($\epsilon_n \simeq \epsilon_m$) points of the energy band. Those points can be seen as the sources of Berry curvature around them. Far from degeneracies, the Berry curvature is rather small causing its shape to be similar to a δ-distribution function. In analogy to electrodynamics, those degeneracy points can be seen as monopoles in the parameter space.

The above discussion is restricted only in the case of a non-degenerate eigenvalue spectrum which is also known as *Abelian* case. If there exists an N-fold degeneracy in the eigenvalues, then one deals with the *non-Abelian* case. In contrast to the Abelian Berry curvature which is a vector, the non-Abelian Berry curvature is a vector-valued matrix in the N-dimensional parameter space. The matrix elements of the non-Abelian Berry curvature are given by

$$\Omega^n_{N,ij}(\boldsymbol{\lambda}) = \partial_{\lambda_i}\mathcal{A}^n_{N,j}(\boldsymbol{\lambda}) - \partial_{\lambda_j}\mathcal{A}^n_{N,i}(\boldsymbol{\lambda}) + [\mathcal{A}^n_{N,i}(\boldsymbol{\lambda}), \mathcal{A}^n_{N,j}(\boldsymbol{\lambda})], \tag{2.21}$$

where for $N = 1$ it is reduced to the Abelian case. The concept of the non-Abelian case is beyond the context of this thesis and so it is no further discussed.

2.3 Berry connection and Berry curvature for Bloch electrons

Moving forward from the introduction of the Berry phase to an abstract quantum system described by a parameter-dependent Hamiltonian, in 1989 Zak [8] proved the occurrence of the Berry phase effect in crystalline solids.

The band structure of a crystal is determined by the single-electron Hamiltonian

$$\hat{\mathcal{H}} = \frac{\hat{\mathbf{p}}^2}{2m} + \hat{V}(\mathbf{r}), \tag{2.22}$$

where $\hat{V}(\mathbf{r}) = \hat{V}(\mathbf{r} + \mathbf{R})$ is the periodic potential and $\mathbf{R}$ is the Bravais lattice vector. The Bloch's theorem implies that the single-electron wavefunctions can be written in the form

$$\psi_{n\mathbf{k}}(\mathbf{r}) = e^{i\mathbf{k}\mathbf{r}} u_{n\mathbf{k}}(\mathbf{r}), \tag{2.23}$$

where $u_{n\mathbf{k}}$ have the periodicity of the lattice

$$u_{n\mathbf{k}}(\mathbf{r}) = u_{n\mathbf{k}}(\mathbf{r} + \mathbf{R}). \tag{2.24}$$

The discrete index n corresponds to the energy bands, while the wavevector $\mathbf{k}$ is restricted inside the Brillouin zone (BZ). Then, over the unit cell, the wavefunctions satisfy the periodic boundary conditions

$$\psi_{n\mathbf{k}}(\mathbf{r} + \mathbf{R}) = e^{i\mathbf{k}\mathbf{R}} \psi_{n\mathbf{k}}(\mathbf{r}). \tag{2.25}$$

At this point, the system does not meet the requirements of the Berry phase theory as it is described by a $\mathbf{k}$-independent Hamiltonian (2.22) and $\mathbf{k}$-dependent boundary conditions (2.25). In order for the Hamiltonian to be $\mathbf{k}$-dependent, the following unitary transformation is made

$$\hat{\mathcal{H}}(\mathbf{k}) = e^{-i\mathbf{k}\mathbf{r}} \hat{\mathcal{H}} e^{i\mathbf{k}\mathbf{r}} = \frac{(\hat{\mathbf{p}} + \hbar\mathbf{k})^2}{2m} + \hat{V}(\mathbf{r}). \tag{2.26}$$

Then, instead of solving the eigenvalue problem

$$\hat{\mathcal{H}} \psi_{n\mathbf{k}}(\mathbf{r}) = \epsilon_{n\mathbf{k}} \psi_{n\mathbf{k}}(\mathbf{r}), \tag{2.27}$$

the following is solved

$$\hat{\mathcal{H}}(\mathbf{k}) u_{n\mathbf{k}}(\mathbf{r}) = \epsilon_{n\mathbf{k}} u_{n\mathbf{k}}(\mathbf{r}). \tag{2.28}$$

The transformed $\hat{\mathcal{H}}(\mathbf{k})$ is also mentioned as the Hamiltonian in crystal momentum representation. The eigenvalue problem (2.27) is now rewritten in terms of an eigenvalue problem of a $\mathbf{k}$-dependent Hamiltonian which can be studied within the Berry phase concept.

If the Brillouin zone is considered as the parameter space of the wavevector $\mathbf{k}$, then from (2.5) the Bloch states pick up a Berry phase

$$\gamma_n = i \oint_{\mathcal{C}} \langle u_{n\mathbf{k}} | \nabla_{\mathbf{k}} u_{n\mathbf{k}} \rangle d\mathbf{k}. \tag{2.29}$$

For non-degenerate Bloch bands n (Abelian case), the corresponding Berry connection according to (2.9) is

$$\boldsymbol{\mathcal{A}}_n(\mathbf{k}) = i\langle u_{n\mathbf{k}}|\nabla_{\mathbf{k}} u_{n\mathbf{k}}\rangle, \tag{2.30}$$

while from (2.13) the corresponding Berry curvature is

$$\boldsymbol{\Omega}_n(\mathbf{k}) = i\langle \nabla_{\mathbf{k}} u_{n\mathbf{k}}| \times |\nabla_{\mathbf{k}} u_{n\mathbf{k}}\rangle. \tag{2.31}$$

As described above, the Bloch states exhibit an inherent Berry phase for the reason that the wavevector $\mathbf{k}$ varies continuously in the Brillouin zone. Berry phase can also appear when $\mathbf{k}$ is perturbed by externally applying small, electric or magnetic, fields. Therefore, the Berry phase concept contributes in the proper description of the dynamics of Bloch electrons.

Chapter 3

The Korringa-Kohn-Rostoker (KKR) Green function method

In 1947 Korringa [9] and in 1954 Kohn and Rostoker [10] introduced the Korringa-Kohn-Rostoker (KKR) multiple scattering method for the calculation of the electronic structure of materials. Firstly, the scattering properties of each atomic scattering site are determined, resulting in a single-site scattering matrix. Then, the multiple scattering by all atoms in the lattice is taken into account, by demanding that the incoming wave at one lattice site equals the sum over the outgoing waves from all other scattering centers. Although, this method was introduced as a wavefunction method, later it was reformulated as a Green function method [11--14]. The Green function of the lattice is being calculated from the Green function of free space via the Dyson equation. The adopted formalism for the KKR Green function method in this thesis is outlined in references [15--22].

3.1 Definition of the Green function

For a quantum mechanical system the Hamiltonian operator in real-spin space is

$$\hat{\mathcal{H}} = \hat{\mathcal{K}} \otimes \hat{\sigma}_0 + \hat{\mathcal{V}} \tag{3.1}$$

where, $\hat{\mathcal{K}}$ is the kinetic energy operator, $\hat{\sigma}_0$ the identity operator in spin space and $\hat{\mathcal{V}}$ the potential operator. For this system, the Green operator is defined as

$$(E - \hat{\mathcal{H}})\hat{\mathcal{G}}(E) = \hat{\mathbb{I}}. \tag{3.2}$$

In terms of the eigenfunctions ψ_i and the eigenergies ϵ_i of $\hat{\mathcal{H}}$, the (retarded) Green function can be expressed in its spectral representation in real-spin space

$$G^{\sigma,\sigma'}(\mathbf{r},\mathbf{r}';E) = \langle \mathbf{r},\sigma|\hat{\mathcal{G}}(E)|\mathbf{r}',\sigma'\rangle = \sum_i \frac{\psi_i^{\sigma}(\mathbf{r})\psi_i^{\sigma'\dagger}(\mathbf{r}')}{E - \epsilon_i + i\Gamma} \tag{3.3}$$

with $\sigma \in \{\uparrow, \downarrow\}$. In the limit of $\Gamma \to 0^+$, the Green function represents an outgoing wave at $\mathbf{r}$, generated by a source at $\mathbf{r}'$. Due to the small imaginary part $i\Gamma$, the Green function has poles for real energies, but is analytic for $\mathrm{Im}E > 0$. For this reason, energy integrals of the Green function converge by a transformation to contour integrals closed in the upper complex energy plane.

From the latter equation, the imaginary part of G can be related to the spectrally space- and spin- resolved density of states $n_\sigma(\mathbf{r}; E)$. After space integration and by using the Dirac identity, the spectral density of states is obtained

$$n_\sigma(\mathbf{r}, E) = -\frac{1}{\pi}\mathrm{Im}G^\sigma(\mathbf{r}, \mathbf{r}; E). \tag{3.4}$$

3.2 The Voronoi construction

In order to calculate the Green function in the KKR formalism a division of the space into atomic cells centered at the nuclei is needed. This is realized by a Voronoi construction which assigns each space point to its closest atomic cell. After this division, the Green function of each atomic cell is being calculated individually. Then, for the full Green function of the crystal, only a connection of all the atomic solutions is needed. The space division is performed by defining a real space vector $\mathbf{x}$ as

$$\mathbf{x} = \mathbf{r} + \mathbf{R}_n, \tag{3.5}$$

where $\mathbf{R}_n$ is a lattice vector and $\mathbf{r}$ is locally defined only within a cell n. The Voronoi construction of the atomic cells and the system of coordinates are shown in Fig.(3.1).

The division into individual atomic cells is also taken into account for the calculation of the crystal potential

$$V(\mathbf{x}) = \sum_n V^n(\mathbf{x} - \mathbf{R}_n), \quad V^n(\mathbf{r}) = \begin{cases} V(\mathbf{r} + \mathbf{R}_n), & \text{if } \mathbf{r} + \mathbf{R}_n \in \text{cell } n \\ 0, & \text{otherwise.} \end{cases} \tag{3.6}$$

For integrals where the the domain of integration is restricted to the volume of the atomic cell, the shape function $\Theta^n(\mathbf{r})$ of each cell is introduced [21]

$$\Theta^n(\mathbf{r}) = \begin{cases} 1, & \text{if } \mathbf{r} + \mathbf{R}_n \in \text{cell } n \\ 0, & \text{otherwise.} \end{cases} \tag{3.7}$$

In systems with more than one atom per unit cell, an additional vector χ_μ is needed to define the position of the μth atom within the unit cell. Then the real space vector is written as

$$\mathbf{x} = \mathbf{r} + \mathbf{R}_n + \boldsymbol{\chi}_\mu \tag{3.8}$$

and the crystal potential as

$$V^{n\mu}(\mathbf{r}) = \begin{cases} V(\mathbf{r} + \mathbf{R}_n + \boldsymbol{\chi}_\mu), & \text{if } \mathbf{r} \in \text{cell } \{n, \mu\} \\ 0, & \text{otherwise.} \end{cases} \tag{3.9}$$

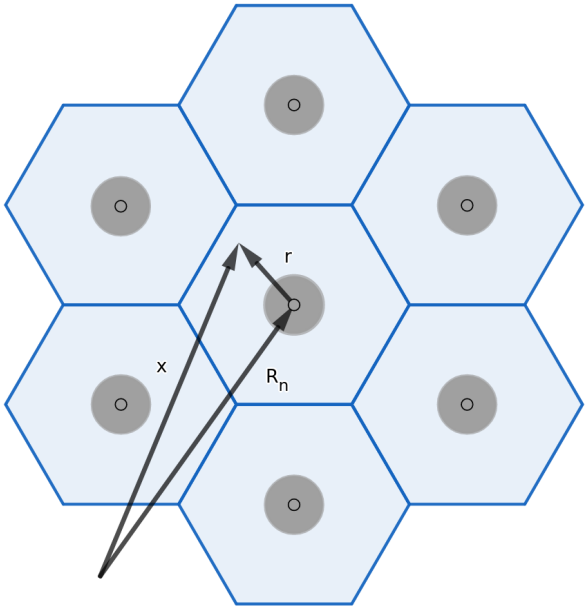

Figure 3.1: *Illustration of the atomic cells (blue lines) found by the Voronoi construction. In the center of the cells the crystal atoms are shown in gray color.*

3.3 Scattering theory

3.3.1 Single-site scattering

First the case of scattering from the potential of a single atom in free space is being studied. The Hamiltonian of the reference potential consists of only the kinetic energy operator. The spin degree of freedom can be neglected for this case because the Hamiltonian is identical for the two spin states. The eigenfunctions of free space are incoming plane waves

$$\phi_{\mathbf{k}}(\mathbf{r}) = \langle \mathbf{r} | \phi_{\mathbf{k}} \rangle = e^{i\mathbf{kr}} \tag{3.10}$$

$$= \sum_L 4\pi i^l j_l(\kappa r) Y_L(\hat{r}) Y_L(\hat{k}). \tag{3.11}$$

The plane waves are expanded in real spherical harmonics $Y_L(\hat{x})$, with expansion coefficients given by the spherical Bessel functions $j_l(x)$. In the angular momentum representation the multiple index $L = (l, m)$ is used, together with $\kappa = |\mathbf{k}| = \sqrt{E_\mathbf{k}}$ in atomic Rydberg units ($\hbar = 1, e^2 = 2, m_e = 1/2, c = 2/\alpha \approx 274$).

The Green function of free space is

$$g(\mathbf{r}, \mathbf{r}'; E) = -\frac{1}{4\pi} \frac{e^{i\kappa|\mathbf{r}-\mathbf{r}'|}}{|\mathbf{r} - \mathbf{r}'|} \tag{3.12}$$

$$= \frac{1}{rr'} \sum_L Y_L(\hat{r}) g_l(\mathbf{r}, \mathbf{r}'; E) Y_L(\hat{r}'). \tag{3.13}$$

The Green function is also expanded in real spherical harmonics, with expansion coefficients defined as

$$g_l(\mathbf{r}, \mathbf{r}'; E) = \kappa r r' \big[\theta(r' - r) j_l(\kappa r) h_l(\kappa r') + \theta(r - r') h_l(\kappa r) j_l(\kappa r')\big], \tag{3.14}$$

where $h_l(\kappa r)$ are the spherical Hankel functions.

If a perturbing potential of finite range $\hat{\mathcal{V}}$ embedded in free space is considered, its representation in real- and spin-space will be

$$V^{\sigma\sigma'}(\mathbf{r}, \mathbf{r}') = \begin{cases} \sum\limits_{L,L'} \dfrac{1}{r^2} V_{LL'}^{\sigma\sigma'}(r) Y_L(\hat{r}) Y_{L'}(\hat{r}') \delta(r - r'), & \text{if } |\mathbf{r}| \le R \\ 0, & \text{if } |\mathbf{r}| > R\,. \end{cases} \tag{3.15}$$

The Lippmann-Schwinger equation for the eigenfunctions of the corresponding Hamiltonian in spinor form is

$$\mathbf{\Psi}_{\mathbf{k},s}(\mathbf{r}) = e^{i\mathbf{k}\mathbf{r}} \boldsymbol{\chi}^s + \int d\mathbf{r}' d\mathbf{r}'' g(\mathbf{r}, \mathbf{r}') \mathbf{V}(\mathbf{r}', \mathbf{r}'') \mathbf{\Psi}_{\mathbf{k},s}(\mathbf{r}''), \tag{3.16}$$

where $s \in \{\uparrow, \downarrow\}$ and $\mathbf{V}(\mathbf{r}', \mathbf{r}'')$ is a (2×2) matrix in spin space. The eigenfunctions $\mathbf{\Psi}_{\mathbf{k},s}(\mathbf{r})$ are (2×1) spinors in Schrödinger-Pauli theory, or (4×1) spinors in Dirac theory.

The eigenfunctions are expanded in real spherical harmonics as [22, 23]

$$\mathbf{\Psi}_{\mathbf{k},s}(\mathbf{r}) = \sum_L 4\pi i^l \mathbf{R}_L^s(\mathbf{r}; E) Y_L(\hat{k}) \tag{3.17}$$

$$\mathbf{R}_L^s(\mathbf{r}; E) = \sum_{L'} \frac{1}{r} \mathbf{R}_{L'L}^s(r; E) Y_{L'}(\hat{r}). \tag{3.18}$$

By replacing the expansions in Eq.(3.16), the Lippmann-Schwinger equations for the scattering solutions are produced

$$\mathbf{R}^s_{L'L}(r;E) = J_L(r;E)\delta_{L',L}\boldsymbol{\chi}^s + \sum_{L''}\int dr'' g_{l'}(r,r'';E)\mathbf{V}_{L'L''}(r'')\mathbf{R}^s_{L''L}(r'';E) \quad (3.19)$$

$$\mathbf{S}^s_{L'L}(r;E) = H_L(r;E)\boldsymbol{\beta}^s_{L'L}(E) + \sum_{L''}\int dr'' g_{l'}(r,r'';E)\mathbf{V}_{L'L''}(r'')\mathbf{S}^s_{L''L}(r'';E), \quad (3.20)$$

where $\boldsymbol{\beta}$ matrix is defined as

$$\boldsymbol{\beta}^s_{L'L}(E) = \delta_{L',L}\boldsymbol{\chi}^s - \kappa\int dr' J_L(r';E)\sum_{L''}\mathbf{V}_{L',L''}(r')\mathbf{S}^s_{L''L}(r';E) \quad (3.21)$$

and the abbreviations $J_L(r;E) = rj_L(\kappa r)$ and $H_L(r;E) = rh_L(\kappa r)$ are used. The scattering functions $R_L(\mathbf{r}), S_L(\mathbf{r})$ are called, respectively, regular (converge when $r \to 0$) and irregular (diverge when $r \to 0$) right solutions of the radial Lippmann-Schwinger equation. They are (2×1) spinors in Schrödinger-Pauli theory, or (4×1) spinors in Dirac theory. Similarly, there exist regular and irregular left solutions, $\bar{R}_L(\mathbf{r})$ and $\bar{S}_L(\mathbf{r})$ respectively [22, 23]

$$\bar{\mathbf{R}}^s_{LL'}(r;E) = \bar{J}_L(r;E)\delta_{L,L'}\boldsymbol{\chi}^s + \sum_{L''}\int dr''\bar{\mathbf{R}}^s_{L''L}(r'';E)\mathbf{V}_{L''L'}(r'')g_{l'}(r'',r;E) \quad (3.22)$$

$$\bar{\mathbf{S}}^s_{LL'}(r;E) = \bar{\boldsymbol{\beta}}^s_{LL'}(E)\bar{H}_L(r;E) + \sum_{L''}\int dr''\bar{\mathbf{S}}^s_{L''L}(r'';E)\mathbf{V}_{L''L'}(r'')g_{l'}(r'',r;E), \quad (3.23)$$

where $\bar{\boldsymbol{\beta}}$ matrix is defined as

$$\bar{\boldsymbol{\beta}}^s_{LL'}(E) = \delta_{L,L'}\boldsymbol{\chi}^s - \kappa\int dr'\bar{\mathbf{R}}^s_{LL''}(r';E)\sum_{L''}\mathbf{V}_{L'',L'}(r')H_{L'}(r';E). \quad (3.24)$$

The left solutions are (1×2) spinors in Schrödinger-Pauli theory, or (1×4) spinors in Dirac theory.

In this scattering problem, the Green function can be expanded in terms of the corresponding right and left scattering solutions, yielding the expression

$$G^s_{LL'}(r,r';E) = \kappa\sum_{L''}\Big[\theta(r'-r)\mathbf{R}^s_{LL''}(r;E)\bar{\mathbf{S}}^s_{L''L'}(r';E) + \theta(r-r')\mathbf{S}^s_{LL''}(r;E)\bar{\mathbf{R}}^s_{L''L'}(r';E)\Big]. \quad (3.25)$$

For the atomic transition matrix (t-matrix), the expression which occurs after expansion into spherical harmonics and integration over the angular part is

$$t^{ss'}_{LL'}(E) = \sum_{\sigma,\sigma'}\sum_{L''}\int dr\delta_{s,\sigma}J_L(r;E)V^{\sigma\sigma'}_{L,L''}(r)R^{\sigma's'}_{L''L'}(r;E). \quad (3.26)$$

3.3.2 Multiple scattering theory

Next the case of multiple scattering from all the atoms within the crystal is studied. A set of identical scatterers at lattice positions $\mathbf{R}_n$, with $n = 1, ..., N$, is considered. The periodic potential is given by

$$V^{\sigma\sigma'}(\mathbf{r} + \mathbf{R}_n, \mathbf{r}' + \mathbf{R}_{n'}) = \delta_{n,n'} V^{\sigma\sigma'}(\mathbf{r}, \mathbf{r}'), \tag{3.27}$$

where $V^{\sigma\sigma'}(\mathbf{r}, \mathbf{r}')$ is the single scattering potential of each identical atomic cell. The following analysis is based on the demand that the incoming wave at site n equals the sum over the scattered waves from all other sites n'.

The expansion coefficients of the Green function of free space for the multiple scattering problem, or also called *structure constants*, are evaluated from

$$g^{nn'}_{\Lambda\Lambda'} = -\delta_{\sigma,\sigma'}(1 - \delta_{n,n'}) 4\pi\kappa \sum_{L''} i^{l-l'+l''} \mathcal{C}_{LL'L''} h_{L''}(\mathbf{R}_n - \mathbf{R}_{n'}; E), \tag{3.28}$$

where the Gaunt coefficients $\mathcal{C}_{LL'L''} = \int d\Omega Y_L(\hat{r}) Y_{L'}(\hat{r}) Y_{L''}(\hat{r})$ and the multiple index $\Lambda = (L, s) = (l, m, s)$ are introduced.

The Green function for the periodic set of identical scatterers has the form [23]

$$G(\mathbf{r} + \mathbf{R}_n, \mathbf{r}' + \mathbf{R}_{n'}; E) = \delta_{n,n'} G^s(\mathbf{r}, \mathbf{r}'; E) + \sum_{\Lambda,\Lambda'} R_\Lambda(\mathbf{r}; E) G^{nn'}_{\Lambda\Lambda'}(E) \bar{R}_{\Lambda'}(\mathbf{r}'; E). \tag{3.29}$$

The first term refers to the single site problem, while the second term refers to the multiple scattering problem. The coefficients $G^{nn'}_{\Lambda\Lambda'}(E)$ are called *structural Green functions* and they are determined, with the help of the structure constants, by the Dyson equation

$$G^{nn'}_{\Lambda\Lambda'}(E) = g^{nn'}_{\Lambda\Lambda'}(E) + \sum_{n'',\Lambda'',\Lambda'''} g^{nn''}_{\Lambda\Lambda''}(E) t^{n''}_{\Lambda''\Lambda'''}(E) G^{n''n'}_{\Lambda'''\Lambda'}(E). \tag{3.30}$$

The physical meaning of the latter equation can be seen if the sum is expanded. An electron can travel from site n' to n directly, or after being scattered by one site, or by two sites, etc.

The generalization to systems with more than one atom in the unit cell is made by introducing the basis vector $\boldsymbol{\chi}_\mu$, with $\mu = 1, ..., N_{at}$, which indicates the position of the μth atom within the unit cell. Then the potential around the cell centers has the form

$$V^{\sigma\sigma'}(\mathbf{r} + \mathbf{R}_n + \boldsymbol{\chi}_\mu, \mathbf{r}' + \mathbf{R}_{n'} + \boldsymbol{\chi}_{\mu'}) = \delta_{n,n'} \delta_{\mu,\mu'} V^{\mu,\sigma\sigma'}(\mathbf{r}, \mathbf{r}'). \tag{3.31}$$

Because of the periodicity of the scatterers, the quantities needed for the determination of the crystal structure depend on the relative position of the scatterers. This becomes evident by a Fourier transformation of the structure constants $g^{\mu\mu'}_{\Lambda\Lambda''}(\mathbf{k}, E)$, which yields an expression that depends only on the geometry of the lattice

$$g^{\mu\mu'}_{\Lambda\Lambda''}(\mathbf{k}, E) = \sum_{n' \neq n} g^{n\mu;n'\mu'}_{\Lambda\Lambda''}(E) e^{i\mathbf{k}\cdot(\mathbf{R}_n + \boldsymbol{\chi}_\mu - \mathbf{R}_{n'} - \boldsymbol{\chi}_{\mu'})} \tag{3.32}$$

The calculation of the structure constants and the t-matrix is performed in $\mathbf{k}$-space for constant energy E, with a cutoff at $l = l_{\max}$. The $l_{\max}$ is determined as the l after which the t-matrix becomes negligible.

The band structure of the crystal $E(\mathbf{k})$ is determined by the *KKR secular equation* [17]

$$\sum_{\Lambda',\mu'} \left[\delta_{\Lambda,\Lambda'}\delta_{\mu,\mu'} - \sum_{\Lambda''} g^{\mu\mu'}_{\Lambda\Lambda''}(\mathbf{k},E)t^{\mu'}_{\Lambda''\Lambda'}(E)\right] C^{\mu'}_{\mathbf{k}\Lambda'} = 0. \tag{3.33}$$

In practice, the secular equation is treated as en eigenvalue problem

$$\bar{\bar{M}}(\mathbf{k},E)\bar{C}_n = \lambda_n \bar{C}_n, \tag{3.34}$$

where the *KKR matrix* is introduced. The band structure points, for which the secular equation is fulfilled, are the pairs $(\mathbf{k},E)$ which correspond to a vanishing eigenvalue $\lambda_n = 0$.

3.3.3 KKR wavefunctions

The Bloch wavefunctions at a certain energy E, in a cell around $\boldsymbol{\chi}_\mu$, that emerge from the KKR multiple scattering theory are

$$\boldsymbol{\Psi}_{n\mathbf{k}}(\mathbf{r}+\boldsymbol{\chi}_\mu) = \sum_{\Lambda} C^{\mu}_{n\mathbf{k}\Lambda} R^{\mu}_{\Lambda}(\mathbf{r};E) \quad \text{for} \quad E_n(\mathbf{k}) = E, \tag{3.35}$$

where n denotes the Bloch band which corresponds to a vanishing eigenvalue.

The normalization of the wavefunctions implies that

$$\langle \boldsymbol{\Psi}_{n\mathbf{k}} | \boldsymbol{\Psi}_{n\mathbf{k}} \rangle = 1. \tag{3.36}$$

From Eq.(3.35) it follows that

$$\langle \boldsymbol{\Psi}_{n\mathbf{k}} | \boldsymbol{\Psi}_{n\mathbf{k}} \rangle = \begin{pmatrix} \Psi^{\uparrow}_{n\mathbf{k}}(\mathbf{r}+\boldsymbol{\chi}_\mu) \\ \Psi^{\downarrow}_{n\mathbf{k}}(\mathbf{r}+\boldsymbol{\chi}_\mu) \end{pmatrix}^{\dagger} \begin{pmatrix} \Psi^{\uparrow}_{n\mathbf{k}}(\mathbf{r}+\boldsymbol{\chi}_\mu) \\ \Psi^{\downarrow}_{n\mathbf{k}}(\mathbf{r}+\boldsymbol{\chi}_\mu) \end{pmatrix} \tag{3.37}$$

$$= \sum_{\sigma}\sum_{\mu} \int_{V^\mu} d\mathbf{r}\, |\Psi^{\sigma}_{n\mathbf{k}}(\mathbf{r}+\boldsymbol{\chi}_\mu)|^2 \tag{3.38}$$

$$= \sum_{\sigma}\sum_{\mu} \int d\mathbf{r}\, \Theta^{\mu}(\mathbf{r}) \Psi^{\sigma *}_{n\mathbf{k}}(\mathbf{r}+\boldsymbol{\chi}_\mu) \Psi^{\sigma}_{n\mathbf{k}}(\mathbf{r}+\boldsymbol{\chi}_\mu), \tag{3.39}$$

where the integration over the volume V^μ of the atomic unit cell at site μ is extended to full space by using the shape functions $\Theta^\mu(\mathbf{r})$. The regular solutions $R^{\sigma s,\mu}_{L}(\mathbf{r};E)$ and the

shape functions are expanded into real spherical harmonics

$$R_L^{\sigma s,\mu}(\mathbf{r};E) = \sum_L \frac{1}{r} R_{L'L}^{\sigma s,\mu}(r;E) Y_{L'}(\hat{r}) \tag{3.40}$$

$$\Theta^{\mu}(\mathbf{r}) = \sum_L \Theta_L^{\mu}(r) Y_L(\hat{r}) \tag{3.41}$$

so, the wavefunctions are expanded as

$$\Psi_{n\mathbf{k}}^{\sigma}(\mathbf{r}+\boldsymbol{\chi}_\mu) = \sum_{L,s} R_L^{\sigma s,\mu}(\mathbf{r};E) C_{\mathbf{k}L}^{s\mu} \tag{3.42}$$

$$= \sum_{L',L,s} \frac{1}{r} R_{L'L}^{\sigma s,\mu}(r;E) Y_{L'}(\hat{r}) C_{\mathbf{k}L}^{s\mu}. \tag{3.43}$$

The normalization equation becomes then [16]

$$\langle \mathbf{\Psi}_{n\mathbf{k}} | \mathbf{\Psi}_{n\mathbf{k}} \rangle = \sum_{\mu} \sum_{ss'} \sum_{LL'} C_{\mathbf{k}L}^{s\mu *} \; \rho_{LL'}^{ss',\mu} \; C_{\mathbf{k}L'}^{s'\mu} \qquad \text{with} \tag{3.44}$$

$$\rho_{LL'}^{ss',\mu}(E) = \sum_{L_1,L_2,L_3} \mathcal{C}_{L_1,L_2,L_3} \int dr \sum_{\sigma} \left[R_{L_1L}^{\sigma s,\mu}(r;E) \right]^* R_{L_2L'}^{\sigma s',\mu}(r;E) \, \Theta_{L_3}(r). \tag{3.45}$$

In practice, the numerical eigenvalue routine that diagonalizes the KKR matrix returns the eigenvectors $\bar{\bar{C}}_{\mathbf{k}}$, which have euclidean norm $\bar{\bar{C}}_{\mathbf{k}}^{\dagger} \bar{\bar{C}}_{\mathbf{k}} = 1$. Those eigenvectors need to be normalized correctly in order for the wavefunctions to fulfill the normalization condition. The correctly normalized eigenvectors are

$$C_{\mathbf{k}L}^{s\mu} = \frac{1}{\sqrt{P}} \tilde{C}_{\mathbf{k}L}^{s\mu} \qquad \text{with} \tag{3.46}$$

$$P = \sum_{\mu} \sum_{ss'} \sum_{LL'} \tilde{C}_{\mathbf{k}L}^{s\mu *} \; \rho_{LL'}^{ss',\mu} \; \tilde{C}_{\mathbf{k}L'}^{s'\mu} = \bar{\bar{C}}_{\mathbf{k}}^{\dagger} \, \bar{\bar{\rho}} \, \bar{\bar{C}}_{\mathbf{k}}. \tag{3.47}$$

The norm P of the wavefunctions is a vector-matrix-vector product. Both P and the matrix $\bar{\bar{\rho}}$ are calculated once per energy. Also $\bar{\bar{\rho}}$ does not depend on $\mathbf{k}$, so it is calculated once for a given energy. For $\bar{\bar{\rho}}$, the spherically symmetric contribution $L_3 = 0$ is calculated separately from the non-spherically symmetric. In that case, the Gaunt coefficients are $\mathcal{C}_{L_1,L_2,0} = \frac{1}{\sqrt{4\pi}} \delta_{L_1,L_2}$ and the shape functions are $\Theta_0^{\mu}(\mathbf{r}) = \sqrt{4\pi}$. So for the spherically symmetric contribution

$$\bar{\bar{\rho}}_{sph}(E) = \sum_{L_1} \frac{1}{\sqrt{4\pi}} \int dr \sum_{\sigma} \left[R_{L_1L}^{\sigma s,\mu}(r;E) \right]^* R_{L_1L'}^{\sigma s',\mu}(r;E) \, \Theta_0(r). \tag{3.48}$$

3.4 Spin-orbit coupling (SOC)

Spin-orbit coupling (SOC) is the relativistic interaction of a particle's spin with its motion inside a potential. In the frame of reference of a moving electron inside the electric field **E** of nucleus, the magnetic field $\mathbf{B} \sim \mathbf{v} \times \mathbf{E}$ which is created, couples to the electron's magnetic moment due to its intrinsic spin. As a purely relativistic effect it is described by the fully relativistic Dirac equation. From this equation, in the non-relativistic limit an additional term is extracted which couples the electron's magnetic moment $\boldsymbol{\sigma}$ to its orbital momentum **L**. That term can be treated as a correction to the Schrödinger equation and is described by the Hamiltonian

$$\hat{\mathcal{H}}_{SOC} = \frac{e\hbar}{4M(r)^2c^2}\frac{1}{r}\frac{dV(r)}{dr}\mathbf{L}\cdot\boldsymbol{\sigma} = \zeta(r)\mathbf{L}\cdot\boldsymbol{\sigma}, \tag{3.49}$$

where $M(r) = m + \frac{1}{2c^2}[E - V(r)]$ is the enhanced relativistic mass close to the core. The factor $\zeta(r)$ is called *spin-orbit coupling parameter* and determines the strength of the spin-orbit coupling. The potential $V(r)$ is the average spin-up and spin-down potential, i.e. $V(r) = \frac{V_\uparrow + V_\downarrow}{2}$. The most important contribution to the potential comes from the strong nuclear electric field and because of that spin-orbit coupling is stronger in heavy atoms. Moreover, the dependence on **L** implies that s-electrons are unaffected by the spin-orbit coupling, whereas p orbitals experience stronger spin-orbit coupling than d or f orbitals because they are closer to the nucleus. The above formalism and details for spin-orbit coupling is based on [24] and Chapters A1 and B6 of Ref. [25].

The total Hamiltonian consists of the Schrödinger equation plus the spin-orbit coupling correction term and it can be seen as a (2×2) matrix in spin-space

$$\begin{pmatrix} \mathcal{H}^{tot}_{\uparrow\uparrow} & \mathcal{H}^{tot}_{\uparrow\downarrow} \\ \mathcal{H}^{tot}_{\downarrow\uparrow} & \mathcal{H}^{tot}_{\downarrow\downarrow} \end{pmatrix} = \begin{pmatrix} \mathcal{H}_{\uparrow\uparrow} & 0 \\ 0 & \mathcal{H}_{\downarrow\downarrow} \end{pmatrix} + \begin{pmatrix} \mathcal{H}^{SOC}_{\uparrow\uparrow} & \mathcal{H}^{SOC}_{\uparrow\downarrow} \\ \mathcal{H}^{SOC}_{\downarrow\uparrow} & \mathcal{H}^{SOC}_{\downarrow\downarrow} \end{pmatrix}. \tag{3.50}$$

For the purpose of numerical experiments, a multiplicative constant is included

$$\hat{\mathcal{H}}_{SOC} \longrightarrow \xi \cdot \hat{\mathcal{H}}_{SOC} \tag{3.51}$$

that may strengthen or weaken the spin-orbit coupling ($\xi = 1$ corresponds to the regular SOC).

Chapter 4

Anomalous Hall effect (AHE)

4.1 Introduction to the origin of AHE

The following review of the aspects of AHE and its origins is based on Refs. [2, 17, 26, 27]. In 1879, E. Hall discovered the *ordinary Hall effect* (HE) [28]. He noticed that the longitudinal current flowing in y-direction through a conductor is curved towards the transverse x-direction, when an external magnetic field H is applied along the vertical z-direction. Due to the Lorentz force, the electrons approach the transverse side of the conductor, generating a finite transverse voltage, also called *Hall voltage*. The resulting *Hall resistivity* ρ_{xy} is proportional to the external magnetic field and can be written as

$$\rho_{xy} = R_0 H_z, \tag{4.1}$$

where R_0 is the *Hall coefficient* which, in the simplest case, is related to the carrier density n as $R_0 = -\frac{1}{ne}$.

Later, in 1880, E. Hall noticed that for ferromagnetic materials the emerging Hall current was larger than in non-magnetic materials [29]. That contribution is known as the *anomalous Hall effect* (AHE). An experimental relation established for the total Hall effect in ferromagnetic materials, with sample magnetization **M** along the z-axis, is

$$\rho_{xy} = R_0 H_z + 4\pi R_s M_z, \tag{4.2}$$

where R_s is the material-dependent coefficient of the anomalous Hall resistivity. The second term is the anomalous contribution which is proportional to the sample magnetization and, usually, is larger than the ordinary contribution.

Although the origin of HE was attributed to the Lorentz force on the moving electrons under magnetic field, the origin of AHE was unknown for years after its discovery. The first successful explanation was given by Karplus and Luttinger in 1954 [30], who stated that the spin-orbit coupling is the mechanism behind AHE. Under the presence of an external electric field, electronic states with spin-orbit coupling acquire a transverse

anomalous velocity. Also, they suggested that the resulting anomalous Hall resistivity is related to the longitudinal resistivity as $\rho_{xy} \propto \rho_{xx}^2$. This contribution is called *intrinsic*, as it depends only on the band structure.

In 1955, Smit proposed the *skew-scattering* as the main mechanism behind AHE [31, 32]. The moving electrons are scattered by the presence of impurities and defects. The spin-orbit coupling causes an asymmetry in the scattering rates of electrons of different spin which creates a preferred average scattering direction, leading to a transverse current. He also stated that this mechanism scales as $\rho_{xy} \propto \rho_{xx}$, in terms of the longitudinal resistivity. In 1970, Berger proposed the *side-jump* mechanism [33] as a contribution to the AHE. According to Berger, the electrons undergo a sudden coordinate shift during scattering by an impurity, leading, also, to an asymmetric scattering process. His mechanism predicts $\rho_{xy} \propto \rho_{xx}^2$, in compliance with the intrinsic contribution. Although it is caused by the impurity scattering, the side-jump mechanism is independent of their concentration. The skew-scattering and the side-jump mechanisms are called *extrinsic* contributions to the AHE, as they are purely impurity and disorder effects.

In the recent years, after the establishment of the Berry phase concept, the study of AHE was promoted significantly. It was understood that the anomalous velocity of the intrinsic mechanism stems from the Berry curvature of the occupied states. The Berry curvature acts as an effective magnetic field in the momentum space which modifies the motion of the electrons, leading to the intrinsic AHE. Thus, it became possible to evaluate the intrinsic AHE from band structure calculations. Studies in ferromagnetic materials and semiconductors came to agreement with experimental results for several materials [34--38]. A more insightful consideration was made by Haldane [39], who stated that the intrinsic contribution to AHE could be calculated from the Berry curvature of quasi-particles on the Fermi surface. Therefore, it is a Fermi surface property and the demanding calculation of the Berry curvature over the entire Fermi sea is not needed. Implementation of Haldane's approach [40] came in agreement with previous theoretical and experimental results.

In conclusion, it is supposed that both the intrinsic and extrinsic contributions in general coexist [41] behind the origin of AHE. In the clean sample limit, the scattering relaxation time is very large and the extrinsic skew-scattering mechanism dominates. The intrinsic contribution is independent of scattering and plays an important role in every occasion. It is most enhanced when the Fermi level is located near avoided crossings of electronic bands due to spin-orbit coupling.

4.2 Semi-classical electronic transport

4.2.1 Equations of motion

The dynamics of Bloch electrons, in the presence of weak external electric **E** or magnetic **B** fields, can be studied under the semi-classical theory, on the wave-packet approach. In this approach, wave-packets are constructed from Bloch states $\psi_{n\mathbf{k}}(\mathbf{r}) = e^{i\mathbf{k}\mathbf{r}}u_{n\mathbf{k}}(\mathbf{r})$, which are the eigenfunctions of the unperturbed lattice Hamiltonian $\hat{\mathcal{H}}_0 = \frac{\hat{\mathbf{p}}^2}{2m} + \hat{V}(\mathbf{r})$, with dispersion relation $\epsilon_n(\mathbf{k})$ for the n-th band. The resulting equations of motion describe how its center of mass $(\mathbf{r}_c, \mathbf{k}_c)$ moves in phase space. The wave-packet is considered strongly centered at $\mathbf{k}_c$, with small **k**-spread compared to the Brillouin zone. On the other hand, the uncertainty principle requires that the **r**-spread is larger than the lattice constant. If the external fields are weak enough, they evolve in space slowly compared to the spread of the wave-packet, and even more slowly compared the lattice constant. In this case, they can be treated as classical perturbations. However, the spatial variations of the periodic potential take place in dimensions much smaller than the spread of the wave-packet, so they are treated in a quantum-mechanical manner. The semi-classical equations of motion which arise under these conditions are

$$\dot{\mathbf{r}}_c = \mathbf{v}_n(\mathbf{k}_c) = \frac{\partial \epsilon_n(\mathbf{k}_c)}{\hbar\, \partial \mathbf{k}_c}, \tag{4.3}$$

$$\hbar\dot{\mathbf{k}}_c = -e\, \mathbf{E} - e\, \dot{\mathbf{r}}_c \times \mathbf{B}. \tag{4.4}$$

The first equation is the common expression for the group velocity of the unperturbed band structure. The second equation describes the dynamics under the influence of the Lorentz force of the external fields. In the presence of constant electric $\mathbf{E} = (0, E_y, 0)$ and magnetic $\mathbf{B} = (0, 0, B_z)$ field, the above equations yield the ordinary Hall resistivity $\rho_{xy} \propto B_z$. However, the above formula fails to explain more complicated phenomena as, for example, the AHE.

In order to derive a more efficient semi-classical formula, it is needed to take into account the presence of the external fields up to first order. The first derivation was successfully made by Chang and Niu [3] and a later generalization was made by Sundaram and Niu [42]. The following analysis is presented in [7]. The wave-packet is constructed from Bloch states as

$$|W_0\rangle = \int_{BZ} d\mathbf{k}\, w(\mathbf{k}, t)|\psi_{n\mathbf{k}}\rangle. \tag{4.5}$$

The weight function $w(\mathbf{k}, t)$ is strongly centered at $\mathbf{k}_c = \int_{BZ} d\mathbf{k}\, |w(\mathbf{k}, t)|^2\mathbf{k}$, and its phase $\arg(w(\mathbf{k}, t))$ must satisfy $\mathbf{r}_c = \langle W_0|\mathbf{r}|W_0\rangle$. With the help of the identity [43]

$$\langle\psi_{n\mathbf{k}'}|\mathbf{r}|\psi_{n\mathbf{k}}\rangle = \delta(\mathbf{k} - \mathbf{k}')\boldsymbol{\mathcal{A}}_n(\mathbf{k}) - i\frac{\partial}{\partial\mathbf{k}}\delta(\mathbf{k} - \mathbf{k}'), \tag{4.6}$$

where $\boldsymbol{\mathcal{A}}_n(\mathbf{k})$ is the Berry connection of the Bloch states, the expectation value of $\mathbf{r}$ in the wave-packet can be written as

$$\begin{aligned}
\mathbf{r}_c &= \langle W_0|\mathbf{r}|W_0\rangle && (4.7)\\
&= \int_{BZ} d\mathbf{k} \int_{BZ} d\mathbf{k}' |w(\mathbf{k},t)||w(\mathbf{k}',t)| \langle \psi_{n\mathbf{k}'}|\mathbf{r}|\psi_{n\mathbf{k}}\rangle e^{i[\arg(w(\mathbf{k},t))-\arg(w(\mathbf{k}',t))]} && (4.8)\\
&\overset{(4.6)}{=} \int_{BZ} d\mathbf{k} \int_{BZ} d\mathbf{k}' |w(\mathbf{k},t)||w(\mathbf{k}',t)| \left[\delta(\mathbf{k}-\mathbf{k}')\boldsymbol{\mathcal{A}}_n(\mathbf{k}) - i\frac{\partial}{\partial \mathbf{k}}\delta(\mathbf{k}-\mathbf{k}')\right] && (4.9)\\
&\quad \times e^{i[\arg(w(\mathbf{k},t))-\arg(w(\mathbf{k}',t))]} && (4.10)\\
&= \int_{BZ} d\mathbf{k} |w(\mathbf{k},t)|^2 \boldsymbol{\mathcal{A}}_n(\mathbf{k}) && (4.11)\\
&\quad + i\int_{BZ} d\mathbf{k} \int_{BZ} d\mathbf{k}' \delta(\mathbf{k}-\mathbf{k}') \frac{\partial}{\partial \mathbf{k}} \left\{ |w(\mathbf{k},t)||w(\mathbf{k}',t)| e^{i[\arg(w(\mathbf{k},t))-\arg(w(\mathbf{k}',t))]} \right\} && (4.12)\\
&= \int_{BZ} d\mathbf{k} |w(\mathbf{k},t)|^2 \boldsymbol{\mathcal{A}}_n(\mathbf{k}) - \int_{BZ} d\mathbf{k} |w(\mathbf{k},t)|^2 \frac{\partial}{\partial \mathbf{k}} \arg(w(\mathbf{k},t)), && (4.13)
\end{aligned}$$

yielding the expression

$$\mathbf{r}_c = \boldsymbol{\mathcal{A}}_n(\mathbf{k}_c) - \frac{\partial}{\partial \mathbf{k}_c} \arg(w(\mathbf{k}_c,t)). \tag{4.14}$$

In general, the equations of motion for $\mathbf{r}_c$ and $\mathbf{k}_c$ can be derived from the time-dependent Schrödinger equation for the wave-packet. The Schrödinger equation can be conveniently obtained by using a time-dependent variational principle (TDVP) from the Lagrangian [44]

$$\mathcal{L} = \left\langle W \middle| i\hbar \frac{d}{dt} \middle| W \right\rangle - \langle W|\hat{\mathcal{H}}|W\rangle, \tag{4.15}$$

where d/dt means the derivative with respect to the time dependence of the wave function explicitly or implicitly through $\mathbf{r}_c$ and $\mathbf{k}_c$. The Hamiltonian $\hat{\mathcal{H}}$ under the presence of electromagnetic fields is

$$\hat{\mathcal{H}} = \frac{1}{2m}\left[\hat{\mathbf{p}} + e\mathbf{A}(\mathbf{r},t)\right]^2 + V(\mathbf{r}) - e\,\phi(\mathbf{r}). \tag{4.16}$$

The vector potential and the scalar potential of the external fields are denoted by $\mathbf{A}$ and ϕ respectively. At the center of the wave-packet, $\mathbf{A}$ can be locally gauged away by the gauge choice

$$|W\rangle = e^{-i\frac{e}{\hbar}\mathbf{A}(\mathbf{r}_c,t)\mathbf{r}}|W_0\rangle. \tag{4.17}$$

Then, the energy of the wave-packet is

$$\langle W|\hat{\mathcal{H}}|W\rangle = \langle W_0|\hat{\mathcal{H}}'|W_0\rangle, \tag{4.18}$$

where

$$\hat{\mathcal{H}}' = e^{i\frac{e}{\hbar}\mathbf{A}(\mathbf{r}_c,t)\mathbf{r}}\,\hat{\mathcal{H}}\,e^{-i\frac{e}{\hbar}\mathbf{A}(\mathbf{r}_c,t)\mathbf{r}} \tag{4.19}$$

$$= \frac{1}{2m}\left\{\hat{\mathbf{p}} + e[\mathbf{A}(\mathbf{r},t) - \mathbf{A}(\mathbf{r}_c,t)]\right\}^2 + V(\mathbf{r}) - e\,\phi(\mathbf{r}). \tag{4.20}$$

For $\mathbf{A}$, the gauge $\mathbf{A}(\mathbf{r},t) = \frac{1}{2}\mathbf{B}\times\mathbf{r} - \mathbf{E}\cdot t$ is chosen, which up to first order in $(\mathbf{r}-\mathbf{r}_c)$ gives

$$\hat{\mathcal{H}}' \simeq \hat{\mathcal{H}}_0 + \frac{e}{4m}\big[\mathbf{B}\times(\mathbf{r}-\mathbf{r}_c)\cdot\hat{\mathbf{p}} + H.c\big] - e\,\phi(\mathbf{r}), \tag{4.21}$$

where $H.c$ denotes the Hermitian conjugate. Therefore, the energy of the wave-packet can be written as

$$\langle W_0|\hat{\mathcal{H}}'|W_0\rangle \simeq \epsilon_n(\mathbf{k}_c) + \frac{e}{2m}\mathbf{B}\cdot\mathbf{L}_n(\mathbf{k}_c) - e\,\phi(\mathbf{r}_c), \tag{4.22}$$

where $\mathbf{L}_n(\mathbf{k}_c) = \langle W_0|(\mathbf{r}-\mathbf{r}_c)\times\hat{\mathbf{p}}|W_0\rangle$ is the orbital angular momentum of the wave-packet about its center of mass $\mathbf{r}_c$. Also, the time derivative term is calculated as

$$\left\langle W\middle|i\hbar\frac{d}{dt}\middle|W\right\rangle = e\,\dot{\mathbf{A}}(\mathbf{r}_c,t)\cdot\mathbf{r}_c - \hbar\frac{\partial}{\partial t}\arg(w(\mathbf{k}_c,t)). \tag{4.23}$$

According to Eq.(4.14) and if total time derivative terms are neglected, the final form for the effective Lagrangian is

$$\mathcal{L}(\mathbf{r}_c,\mathbf{k}_c,\dot{\mathbf{r}}_c,\dot{\mathbf{k}}_c,t) = \hbar\,\mathbf{k}_c\cdot\dot{\mathbf{r}}_c - e\,\dot{\mathbf{r}}_c\cdot\mathbf{A}(\mathbf{r}_c,t) + \hbar\,\dot{\mathbf{k}}_c\cdot\boldsymbol{\mathcal{A}}_n(\mathbf{k}_c) + e\,\phi(\mathbf{r}_c) - E_n(\mathbf{k}_c), \tag{4.24}$$

where the unperturbed band energy $\epsilon_n(\mathbf{k}_c)$ is modified by the magnetization energy $\frac{e}{2m}\mathbf{B}\cdot\mathbf{L}_n(\mathbf{k}_c)$, leading to a total band energy $E_n(\mathbf{k}_c) = \epsilon_n(\mathbf{k}_c) + \frac{e}{2m}\mathbf{B}\cdot\mathbf{L}_n(\mathbf{k}_c)$.

Finally, the equations of motion are derived from the Euler-Lagrange equations

$$\frac{d}{dt}\left(\frac{\partial\mathcal{L}}{\partial\dot{\mathbf{r}}_c}\right) - \frac{\partial\mathcal{L}}{\partial\mathbf{r}_c} = 0 \quad\text{and}\quad \frac{d}{dt}\left(\frac{\partial\mathcal{L}}{\partial\dot{\mathbf{k}}_c}\right) - \frac{\partial\mathcal{L}}{\partial\mathbf{k}_c} = 0, \tag{4.25}$$

resulting to

$$\dot{\mathbf{r}}_c = \frac{\partial E_n(\mathbf{k}_c)}{\hbar\,\partial\mathbf{k}_c} - \dot{\mathbf{k}}_c\times\boldsymbol{\Omega}_n(\mathbf{k}_c), \tag{4.26}$$

$$\hbar\,\dot{\mathbf{k}}_c = -e\,\mathbf{E} - e\,\dot{\mathbf{r}}_c\times\mathbf{B}, \tag{4.27}$$

where $\boldsymbol{\Omega}_n$ is the Berry curvature of the Bloch states. It is clear that, compared to (4.3), the expression for the velocity contains also the *anomalous velocity* term and the modification of the band energy due to the magnetization energy.

In the case of a ferromagnet subject to a constant external electric field **E** and in the absence of magnetic field **B**, the latter equations of motion can be written as

$$\dot{\mathbf{r}}_c = \frac{\partial \epsilon_n(\mathbf{k}_c)}{\hbar\, \partial \mathbf{k}_c} + \frac{e}{\hbar}\mathbf{E} \times \mathbf{\Omega}_n(\mathbf{k}_c), \tag{4.28}$$

$$\hbar\, \dot{\mathbf{k}}_c = -e\, \mathbf{E}, \tag{4.29}$$

where the anomalous velocity is $\mathbf{v}_n^a(\mathbf{k}_c) = \frac{e}{\hbar}\mathbf{E} \times \mathbf{\Omega}_n(\mathbf{k}_c)$. This term is transverse to the electric field and gives rise to the intrinsic AHE. Going beyond Karplus and Luttinger, the semi-classical description can describe how the intrinsic AHE stems from the Berry curvature of the Bloch states.

4.2.2 Electron transport

The electron transport in solids can be described by the Boltzmann equation within the semi-classical approach. The Boltzmann equation determines the evolution of the non-equilibrium *distribution function* $g = g(\mathbf{r}, \mathbf{k}, t)$ of Bloch electrons, which are accelerated by external fields. The total rate of change for g is written as

$$\frac{dg}{dt} = \frac{\partial g}{\partial t} + \dot{\mathbf{r}} \cdot \frac{\partial g}{\partial \mathbf{r}} + \dot{\mathbf{k}} \cdot \frac{\partial g}{\partial \mathbf{k}}. \tag{4.30}$$

The changes in g are caused by the semi-classical dynamics and, also, by collisions at impurities or phonons. In the steady state, the total rate of change must be equal to the collision term, i.e. $\frac{dg}{dt} = \left(\frac{\partial g}{\partial t}\right)_{coll}$. Therefore, in the relaxation time approximation for the collisions, i.e. $g - f = Ae^{t/\tau}$ the steady state g obeys the Boltzmann equation [7, 45]

$$\dot{\mathbf{r}} \cdot \frac{\partial g_{n\mathbf{k}}}{\partial \mathbf{r}} + \dot{\mathbf{k}} \cdot \frac{\partial g_{n\mathbf{k}}}{\partial \mathbf{k}} = \frac{f_{n\mathbf{k}} - g_{n\mathbf{k}}}{\tau_{n\mathbf{k}}}, \tag{4.31}$$

where $\tau_{n\mathbf{k}}$ is the relaxation time and $f_{n\mathbf{k}}$ is the Fermi-Dirac equilibrium distribution function of the Bloch state $\mathbf{k}$, with band index n.

In order to describe the intrinsic AHE, the presence of a constant electric field **E** is considered. The center of mass $(\mathbf{r}_c, \mathbf{k}_c)$ of the wave-packet constructed in 4.2.1 is further simply denoted as $(\mathbf{r}, \mathbf{k})$. Then, up to first order in **E**, the solution of (4.31) gives

$$g_{n\mathbf{k}} = f_{n\mathbf{k}} + \tau_{n\mathbf{k}} \frac{e}{\hbar}\, \mathbf{E} \cdot \frac{\partial \epsilon_n}{\partial \mathbf{k}} \frac{\partial f_{n\mathbf{k}}}{\partial \epsilon_n}. \tag{4.32}$$

According to the linear response theory, the charge conductivity tensor σ_c is defined as

$$\mathbf{J}_c = \bar{\bar{\sigma}}_c \mathbf{E}. \tag{4.33}$$

The electric current density is given by

$$\mathbf{J}_c = -\frac{e}{V}\sum_{n,\mathbf{k}} g_{n\mathbf{k}}\,\mathbf{v}_{n\mathbf{k}} \tag{4.34}$$

$$= -\frac{e}{VV_{BZ}}\sum_{n}\int_{BZ} d\mathbf{k}\, g_{n\mathbf{k}}\,\mathbf{v}_{n\mathbf{k}} \tag{4.35}$$

$$= -\frac{e}{(2\pi)^3}\sum_{n}\int_{BZ} d\mathbf{k}\, g_{n\mathbf{k}}\,\mathbf{v}_{n\mathbf{k}}, \tag{4.36}$$

where V is the crystal volume, V_{BZ} is the Brillouin zone volume and $\mathbf{v}_{n\mathbf{k}}$ is the electron velocity which is given by the term $\dot{\mathbf{r}}_c$ in (4.28). By inserting the semi-classical equations of motion (4.28) and up to first order in $\mathbf{E}$, the resulting expression for the electric current density is

$$\mathbf{J}_c = -\mathbf{E}\times\frac{e^2}{\hbar(2\pi)^3}\sum_{n}\int_{BZ} d\mathbf{k}\, f_{n\mathbf{k}}\,\boldsymbol{\Omega}_n(\mathbf{k}) - \frac{e^2\tau}{(2\pi)^3}\sum_{n}\int_{BZ} d\mathbf{k}\frac{\partial\epsilon_n}{\partial\mathbf{k}}\mathbf{E}\cdot\frac{\partial\epsilon_n}{\partial\mathbf{k}}\frac{\partial f_{n\mathbf{k}}}{\partial\epsilon_n}, \tag{4.37}$$

with the approximation $\tau_{n\mathbf{k}} = \tau = \text{const.}$

An expression for the conductivity tensor can be deduced from (4.37), in combination with (4.33). The second term of (4.37) yields the symmetric conductivity tensor, which depends on the properties of the system near the Fermi energy. The first term of (4.37) gives the anti-symmetric conductivity tensor

$$\varepsilon_{ijk}\sigma^c_{ij} = -\frac{e^2}{\hbar(2\pi)^3}\sum_{n}\int_{BZ} d\mathbf{k}\, f_{n\mathbf{k}}\,\Omega^k_n(\mathbf{k}), \quad \text{where} \quad (i,j,k) = \{x,y,z\}. \tag{4.38}$$

Thus, the modern view on the origin of the anomalous Hall effect and the *spin Hall effect* (SHE) can be summarized as follows [46]. In ferromagnetic systems, where the time-reversal symmetry is broken and the space-inversion symmetry is present, the non-vanishing total Berry curvature of the occupied Bloch states $\boldsymbol{\Omega}(\mathbf{k}) = \sum_n \boldsymbol{\Omega}_n(\mathbf{k})$ creates a transverse charge current for each spin direction. If the magnetization is finite $\mathbf{M} \neq 0$, the number of spin-up electrons differs from the number of spin-down electrons, leading to a non-vanishing total transverse charge current. Hence, this is the mechanism behind the origin of the intrinsic AHE. The intrinsic anomalous conductivity can be calculated by (4.38). On the other hand, in non-magnetic systems, where the time-reversal symmetry exists but the space-inversion symmetry is broken, the total Berry curvature vanishes. The number of spin-up electrons equals the number of spin-down electrons and the magnetization is zero. In this case, the charge current vanishes but there exist a spin current, which gives rise to the SHE. A schematic representation of both AHE and SHE can be seen in Fig.(4.1). In the context of this thesis, only ferromagnetic systems are studied, so focus is given only in the intrinsic AHE calculation.

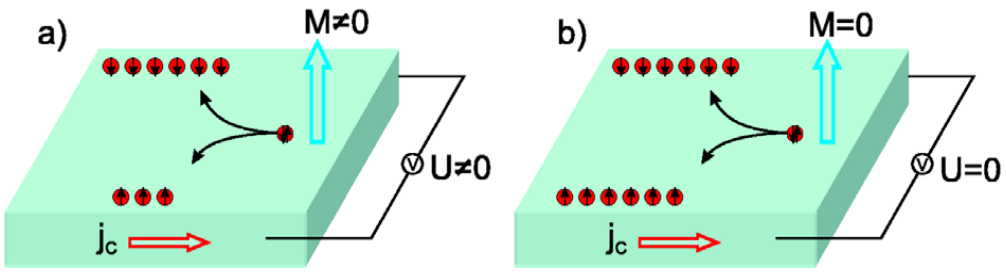

Figure 4.1: *Illustration of (a) the anomalous Hall effect and (b) the spin Hall effect [46].*

Chapter 5

First-principles calculation of the Berry curvature for Bloch electrons

As seen in Chapter 4, the first-principles calculation of the Berry curvature of Bloch states is crucial in order to study charge or spin transport phenomena as AHE and SHE. The two most common approaches to calculate the Berry curvature involve the Kubo-formula [36, 47, 48] and the Wannier interpolation scheme [37, 40]. A new approach within the KKR framework was implemented by Gradhand et al. [4]. This approach is the subject of this thesis. In contrast with Gradhand et al., two different considerations are made. The first one is that the Bloch wavefunctions are treated as solutions of the full-potential scalar relativistic approximation to the Dirac equation, with the addition of a correction representing the SOC, while Gradhand et al. treat the Dirac equation in the atomic-sphere approximation (ASA). The second one is that a different choice for the normalization of the scattering solutions is made. As a consequence, there is distinction in the resulting equations for the Abelian Berry connection and the Abelian Berry curvature, leading to a numerical differentiation of the eigenvectors of the KKR matrix. The new form of the Abelian Berry curvature is later used to calculate the intrinsic anomalous hall conductivity (AHC).

5.1 The KKR framework and the group velocity of Bloch states

The following discussion is restricted to ferromagnetic systems with one atom per unit cell. In such systems, the spontaneous magnetization breaks the time-reversal degeneracy of the Bloch bands. Then, because the Bloch states are non-degenerate, one deals with the Abelian case for the Berry phase.

As seen in Chapter 3, the KKR expansion for the wavefunction is

$$\Psi_{n\mathbf{k}}(\mathbf{r}) = \sum_{\Lambda} C^{n}_{\Lambda}(\mathbf{k})\, R_{\Lambda}(E_n(\mathbf{k}); \mathbf{r}), \tag{5.1}$$

where R_Λ are the regular scattering solutions, C^n_Λ are the right eigenvectors of the KKR matrix and $\Lambda = (L, s) = (l, m, s)$ is a multiple index introduced to label the spin and orbital angular momentum quantum numbers. The band structure of the lattice, i.e the energy eigenvalues $E_n(\mathbf{k})$, is determined by the solution of the eigenvalue problem of the KKR matrix

$$\bar{\bar{M}}(\mathbf{k}, E)\bar{C}_n = \lambda_n \bar{C}_n. \tag{5.2}$$

The band structure points are the combinations $(\mathbf{k}, E)$ which correspond to a vanishing eigenvalue $\lambda_n = 0$. The KKR matrix is defined as

$$M_{\Lambda,\Lambda'}(\mathbf{k}, E) = \delta_{\Lambda,\Lambda'} - \sum_{\Lambda''} g_{\Lambda\Lambda''}(\mathbf{k}, E)\, t_{\Lambda''\Lambda'}(E), \tag{5.3}$$

where $g_{\Lambda\Lambda''}(\mathbf{k}, E)$ are the structure constants, which depend only on the geometry of the lattice, and $t_{\Lambda''\Lambda'}(E)$ is the t-matrix, which depends only on the shape of the scattering periodic potential. Also, the KKR matrix has a dimension of $N \times N$, where $N = 2(l_{max} + 1)^2$ and the factor 2 accounts for the spin-up and spin-down directions. The KKR matrix is a non-Hermitian matrix, so apart from the right eigenvectors $\bar{C}_n$, for the same eigenvalue λ_n, there exist also the distinct left eigenvectors $\bar{D}_n$ which are defined as

$$\bar{D}^{\dagger}_n \bar{\bar{M}}(\mathbf{k}, E) = \lambda_n \bar{D}^{\dagger}_n. \tag{5.4}$$

If the normalization condition

$$\bar{C}^{\dagger}_n \bar{C}_n = 1 \quad \text{and} \quad \bar{D}^{\dagger}_n \bar{D}_n = 1, \tag{5.5}$$

is used, then the eigenvectors also fulfill

$$\bar{D}^{\dagger}_n \bar{C}_{n'} \propto \delta_{n,n'}, \quad \bar{D}^{\dagger}_n \bar{C}_n \neq 1, \tag{5.6}$$

$$\bar{C}^{\dagger}_n \bar{C}_{n'} \neq 0, \quad \bar{D}^{\dagger}_n \bar{D}_{n'} \neq 0. \tag{5.7}$$

An expression for the group velocity of the Bloch states can be obtained in terms of the properties of the KKR matrix. Starting from the fact that the band structure points obey the condition $\lambda_n(\mathbf{k}, E_n(\mathbf{k})) = 0$, the total derivative of the eigenvalues, which is normal to the constant energy surface $E = E_n(\mathbf{k})$, gives

$$\nabla_{\mathbf{k}} \lambda_n(\mathbf{k}, E)\Big|_{E=E_n(\mathbf{k})} = 0 \Rightarrow \tag{5.8}$$

$$\frac{\partial \lambda_n(\mathbf{k}, E)}{\partial \mathbf{k}}\bigg|_{E=E_n(\mathbf{k})} + \nabla_{\mathbf{k}} E_n(\mathbf{k}) \frac{\partial \lambda_n(\mathbf{k}, E)}{\partial E}\bigg|_{E=E_n(\mathbf{k})} = 0. \tag{5.9}$$

It should be noticed that the total derivative $\nabla_{\mathbf{k}}$ is restricted to the band structure points $\mathbf{k}$ which constitute the constant energy surface $E = E_n(\mathbf{k})$. Then, the definition of the group velocity yields

$$\mathbf{v}_n(\mathbf{k}) = \frac{1}{\hbar}\nabla_{\mathbf{k}} E_n(\mathbf{k}) = -\frac{1}{\hbar}\frac{\left.\dfrac{\partial \lambda_n(\mathbf{k}, E)}{\partial \mathbf{k}}\right|_{E=E_n(\mathbf{k})}}{\left.\dfrac{\partial \lambda_n(\mathbf{k}, E)}{\partial E}\right|_{E=E_n(\mathbf{k})}}. \tag{5.10}$$

From the definition of the left eigenvectors, the following expression can be obtained

$$\bar{D}_n^{\dagger}\bar{\bar{M}}\bar{C}_n = \lambda_n \bar{D}_n^{\dagger}\bar{C}_n. \tag{5.11}$$

By taking the partial derivative of both sides with respect to $\mathbf{k}$, one takes

$$\frac{\partial \lambda_n(\mathbf{k}, E)}{\partial \mathbf{k}} = \frac{\bar{D}_n^{\dagger}(\partial \bar{\bar{M}}/\partial \mathbf{k})\bar{C}_n}{\bar{D}_n^{\dagger}\bar{C}_n}. \tag{5.12}$$

Therefore, the group velocity is given by the expression

$$\mathbf{v}_n(\mathbf{k}) = -\frac{1}{\hbar}\frac{\bar{D}_n^{\dagger}\left.\dfrac{\partial \bar{\bar{M}}(\mathbf{k}, E)}{\partial \mathbf{k}}\right|_{E=E_n(\mathbf{k})}\bar{C}_n}{\left(\bar{D}_n^{\dagger}\bar{C}_n\right)\left.\dfrac{\partial \lambda_n(\mathbf{k}, E)}{\partial E}\right|_{E=E_n(\mathbf{k})}}. \tag{5.13}$$

The partial derivative $\partial\lambda_n(\mathbf{k}, E)/\partial E$ is calculated numerically, while the partial derivative $\partial\bar{\bar{M}}/\partial\mathbf{k}$ is calculated from the relation

$$\frac{\partial \bar{\bar{M}}(\mathbf{k}, E_n(\mathbf{k}))}{\partial \mathbf{k}} = -\frac{\partial \bar{\bar{g}}(\mathbf{k}, E_n(\mathbf{k}))}{\partial \mathbf{k}}\, t(E_n(\mathbf{k})), \tag{5.14}$$

where

$$\frac{\partial \bar{\bar{g}}(\mathbf{k}, E_n(\mathbf{k}))}{\partial \mathbf{k}} = i \sum_{\mathbf{R}} \mathbf{R}\, e^{i\mathbf{k}\mathbf{R}}\, \bar{\bar{g}}(\mathbf{R}, E_n(\mathbf{k})). \tag{5.15}$$

The former relation is derived by taking the partial derivative of the KKR matrix with respect to $\mathbf{k}$, while the latter relation is expressed in terms of the real-space structure constants $\bar{\bar{g}}(\mathbf{R}, E_n(\mathbf{k}))$ and is derived from the derivative of (3.32).

5.2 Abelian Berry connection

In Section 2.3 the Berry phase concept for the Bloch states of a crystalline solid was introduced. It was shown that the Berry connection is expressed as (2.30)

$$\boldsymbol{\mathcal{A}}_n(\mathbf{k}) = i\langle u_{n\mathbf{k}}|\nabla_{\mathbf{k}} u_{n\mathbf{k}}\rangle = i\int_{\omega} u_{n\mathbf{k}}^{\dagger}(\mathbf{r})\nabla_{\mathbf{k}} u_{n\mathbf{k}}(\mathbf{r})d\mathbf{r}, \tag{5.16}$$

where ω is the volume of a unit cell. Because the KKR method calculates the wavefunction $\Psi_{n\mathbf{k}}(\mathbf{r})$ and not the periodic part $u_{n\mathbf{k}}(\mathbf{r})$, the above expression for $\boldsymbol{\mathcal{A}}_n(\mathbf{k})$ needs to be reformulated in terms of $\Psi_{n\mathbf{k}}(\mathbf{r})$. This can be done with the help of $u_{n\mathbf{k}}(\mathbf{r}) = e^{-i\mathbf{k}\mathbf{r}}\Psi_{n\mathbf{k}}(\mathbf{r})$. The resulting expression for the Berry connection is [4]

$$\boldsymbol{\mathcal{A}}_n(\mathbf{k}) = i\int_\omega \Psi^\dagger_{n\mathbf{k}}(\mathbf{r})\nabla_{\mathbf{k}}\Psi_{n\mathbf{k}}(\mathbf{r})d\mathbf{r} + \int_\omega \Psi^\dagger_{n\mathbf{k}}(\mathbf{r})\mathbf{r}\Psi_{n\mathbf{k}}(\mathbf{r})d\mathbf{r} = \boldsymbol{\mathcal{A}}^k_n(\mathbf{k}) + \boldsymbol{\mathcal{A}}^r_n(\mathbf{k}), \quad (5.17)$$

where

$$\boldsymbol{\mathcal{A}}^k_n(\mathbf{k}) = i\int_\omega \Psi^\dagger_{n\mathbf{k}}(\mathbf{r})\nabla_{\mathbf{k}}\Psi_{n\mathbf{k}}(\mathbf{r})d\mathbf{r}, \quad (5.18)$$

and

$$\boldsymbol{\mathcal{A}}^r_n(\mathbf{k}) = \int_\omega \Psi^\dagger_{n\mathbf{k}}(\mathbf{r})\ \mathbf{r}\ \Psi_{n\mathbf{k}}(\mathbf{r})d\mathbf{r}. \quad (5.19)$$

The total derivative of the KKR expansion (5.1) which is normal to the constant energy surface $E = E_n(\mathbf{k})$ is

$$\nabla_{\mathbf{k}}\Psi_{n\mathbf{k}}(\mathbf{r}) = \sum_\Lambda \left[\nabla_{\mathbf{k}}C^n_\Lambda(\mathbf{k})\ R_\Lambda(E;\mathbf{r}) + C^n_\Lambda(\mathbf{k})\ \mathbf{v}_n(\mathbf{k})\ \frac{\partial R_\Lambda(E;\mathbf{r})}{\partial E}\right], \quad (5.20)$$

which gives

$$\langle\Psi_{n\mathbf{k}}|\nabla_{\mathbf{k}}\Psi_{n\mathbf{k}}\rangle = \sum_{\Lambda,\Lambda'} C^{n*}_\Lambda(\mathbf{k})\ \nabla_{\mathbf{k}}C^n_{\Lambda'}(\mathbf{k})\int_\omega R^\dagger_\Lambda(E;\mathbf{r})\ R_{\Lambda'}(E;\mathbf{r})\ d\mathbf{r} \quad (5.21)$$

$$+\ \mathbf{v}_n(\mathbf{k})\ \sum_{\Lambda,\Lambda'} C^{n*}_\Lambda(\mathbf{k})\ C^n_{\Lambda'}(\mathbf{k})\int_\omega R^\dagger_\Lambda(E;\mathbf{r})\ \frac{\partial R_{\Lambda'}(E;\mathbf{r})}{\partial E}\ d\mathbf{r}. \quad (5.22)$$

Then, $\boldsymbol{\mathcal{A}}^k_n(\mathbf{k})$ can be written as

$$\boldsymbol{\mathcal{A}}^k_n(\mathbf{k}) = \boldsymbol{\mathcal{A}}^{KKR}_n(\mathbf{k}) + \boldsymbol{\mathcal{A}}^v_n(\mathbf{k}), \quad (5.23)$$

where

$$\boldsymbol{\mathcal{A}}^{KKR}_n(\mathbf{k}) = i\ \bar{C}^\dagger_n\ \bar{\bar{\rho}}\ \nabla_{\mathbf{k}}\bar{C}_n, \quad (5.24)$$

with the matrix $\bar{\bar{\rho}}$ given by

$$(\bar{\bar{\rho}})_{\Lambda,\Lambda'}(E) = \int_\omega R^\dagger_\Lambda(E;\mathbf{r})\ R_{\Lambda'}(E;\mathbf{r})\ d\mathbf{r} \quad (5.25)$$

and

$$\boldsymbol{\mathcal{A}}^v_n(\mathbf{k}) = i\ \mathbf{v}_n\ \bar{C}^\dagger_n\ \bar{\bar{\Delta}}\ \bar{C}_n, \quad (5.26)$$

with the matrix $\bar{\bar{\Delta}}$ given by

$$\left(\bar{\bar{\Delta}}\right)_{\Lambda,\Lambda'}(E) = \int_{\omega} R^{\dagger}_{\Lambda}(E;\mathbf{r})\,\frac{\partial R_{\Lambda'}(E;\mathbf{r})}{\partial E}\,d\mathbf{r}. \tag{5.27}$$

For $\boldsymbol{\mathcal{A}}^{r}_{n}(\mathbf{k})$, the expansion (5.1) yields

$$\boldsymbol{\mathcal{A}}^{r}_{n}(\mathbf{k}) = \bar{C}^{\dagger}_{n}\,\bar{\bar{\mathbf{r}}}\,\bar{C}_{n}, \tag{5.28}$$

where the vector matrix $\bar{\bar{\mathbf{r}}}$ is introduced as

$$(\bar{\bar{\mathbf{r}}})_{\Lambda,\Lambda'}(E) = \int_{\omega} R^{\dagger}_{\Lambda}(E;\mathbf{r})\;\mathbf{r}\;R_{\Lambda'}(E;\mathbf{r})\,d\mathbf{r}. \tag{5.29}$$

Therefore, the full expression for the Berry connection is

$$\boldsymbol{\mathcal{A}}_{n}(\mathbf{k}) = \boldsymbol{\mathcal{A}}^{KKR}_{n}(\mathbf{k}) + \boldsymbol{\mathcal{A}}^{v}_{n}(\mathbf{k}) + \boldsymbol{\mathcal{A}}^{r}_{n}(\mathbf{k}). \tag{5.30}$$

5.3 Abelian Berry curvature

Since the Berry curvature is defined as

$$\boldsymbol{\Omega}_{n}(\mathbf{k}) = \nabla_{\mathbf{k}} \times \boldsymbol{\mathcal{A}}_{n}(\mathbf{k}), \tag{5.31}$$

it can be also considered as a sum of the same contributions as the Berry connection

$$\boldsymbol{\Omega}_{n}(\mathbf{k}) = \boldsymbol{\Omega}^{KKR}_{n}(\mathbf{k}) + \boldsymbol{\Omega}^{v}_{n}(\mathbf{k}) + \boldsymbol{\Omega}^{r}_{n}(\mathbf{k}). \tag{5.32}$$

For the following calculations, the completeness relation of the non-Hermitian KKR matrix is taken into consideration

$$\sum_{m=1}^{N} \frac{\bar{C}_{m}\bar{D}^{\dagger}_{m}}{\bar{D}^{\dagger}_{m}\bar{C}_{m}} = \sum_{m=1}^{N} \frac{\bar{D}_{m}\bar{C}^{\dagger}_{m}}{\bar{C}^{\dagger}_{m}\bar{D}_{m}} = \bar{\bar{\mathbf{1}}}, \tag{5.33}$$

together with the vector calculus identity

$$\nabla \times (\psi\mathbf{A}) = \psi(\nabla \times \mathbf{A}) + \nabla\psi \times \mathbf{A}, \tag{5.34}$$

where ψ is a scalar quantity and $\mathbf{A}$ a vector.

Starting from the component $\mathbf{\Omega}_n^{KKR}(\mathbf{k})$, one gets

$$\mathbf{\Omega}_n^{KKR}(\mathbf{k}) = \nabla_{\mathbf{k}} \times \boldsymbol{\mathcal{A}}_n^{KKR}(\mathbf{k}) = i\,\nabla_{\mathbf{k}}\big(\bar{C}_n^{\dagger}\,\bar{\bar{\rho}}\,\big) \times \nabla_{\mathbf{k}}\bar{C}_n + i\,\bar{C}_n^{\dagger}\,\bar{\bar{\rho}}\,\underbrace{\big(\nabla_{\mathbf{k}} \times \nabla_{\mathbf{k}}\bar{C}_n\big)}_{=0} \tag{5.35}$$

$$= i \sum_{\Lambda,\Lambda'} \int \nabla_{\mathbf{k}} \left(C_{\Lambda}^{n*}\, R_{\Lambda}^{\dagger}\, R_{\Lambda'}\right) \times \nabla_{\mathbf{k}} C_{\Lambda'}^{n}\, d\mathbf{r} \tag{5.36}$$

$$= i \sum_{\Lambda,\Lambda'} \int \Bigg(\nabla_{\mathbf{k}} C_{\Lambda}^{n*}\, R_{\Lambda}^{\dagger}\, R_{\Lambda'} + \mathbf{v}_n\, C_{\Lambda}^{n*}\, \frac{\partial R_{\Lambda}^{\dagger}}{\partial E} R_{\Lambda'} \tag{5.37}$$

$$+ \mathbf{v}_n\, C_{\Lambda}^{n*}\, R_{\Lambda}^{\dagger}\, \frac{\partial R_{\Lambda'}}{\partial E} \Bigg) \times \nabla_{\mathbf{k}} C_{\Lambda'}^{n}\, d\mathbf{r} \tag{5.38}$$

$$= i \left(\nabla_{\mathbf{k}} \bar{C}_n^{\dagger}\, \bar{\bar{\rho}} + \mathbf{v}_n\, \bar{C}_n^{\dagger}\, \bar{\bar{\Delta}}^{\dagger} + \mathbf{v}_n\, \bar{C}_n^{\dagger}\, \bar{\bar{\Delta}} \right) \times \nabla_{\mathbf{k}} \bar{C}_n \tag{5.39}$$

$$= i\,\nabla_{\mathbf{k}} \bar{C}_n^{\dagger}\, \bar{\bar{\rho}} \times \nabla_{\mathbf{k}} \bar{C}_n + i\,\mathbf{v}_n \times \Big(\bar{C}_n^{\dagger}\, \bar{\bar{\Delta}}\, \nabla_{\mathbf{k}} \bar{C}_n + \bar{C}_n^{\dagger}\, \bar{\bar{\Delta}}^{\dagger}\, \nabla_{\mathbf{k}} \bar{C}_n \Big). \tag{5.40}$$

In order to avoid the matrix-matrix cross products of the last equation, the completeness relation (5.33) is used, yielding to

$$\mathbf{\Omega}_n^{KKR}(\mathbf{k}) = i \sum_m \frac{\nabla_{\mathbf{k}} \bar{C}_n^{\dagger}\, \bar{\bar{\rho}}\, \bar{C}_m \times \bar{D}_m^{\dagger}\, \nabla_{\mathbf{k}} \bar{C}_n}{\bar{D}_m^{\dagger}\, \bar{C}_m} + i\,\mathbf{v}_n \times \Big(\bar{C}_n^{\dagger}\, \bar{\bar{\Delta}}\, \nabla_{\mathbf{k}} \bar{C}_n + \bar{C}_n^{\dagger}\, \bar{\bar{\Delta}}^{\dagger}\, \nabla_{\mathbf{k}} \bar{C}_n \Big), \tag{5.41}$$

where the sum is going over all the eigenstates of the KKR matrix. At last, the component $\mathbf{\Omega}_n^{KKR}(\mathbf{k})$ is given by

$$\mathbf{\Omega}_n^{KKR}(\mathbf{k}) = i \sum_m \frac{\big(\bar{C}_m^{\dagger}\, \bar{\bar{\rho}}\, \nabla_{\mathbf{k}} \bar{C}_n\big)^* \times \bar{D}_m^{\dagger}\, \nabla_{\mathbf{k}} \bar{C}_n}{\bar{D}_m^{\dagger}\, \bar{C}_m} + i\,\mathbf{v}_n \times \big(\bar{C}_n^{\dagger}\, \bar{\bar{\Delta}}\, \nabla_{\mathbf{k}} \bar{C}_n + \bar{C}_n^{\dagger}\, \bar{\bar{\Delta}}^{\dagger}\, \nabla_{\mathbf{k}} \bar{C}_n \big). \tag{5.42}$$

Next, the component $\mathbf{\Omega}_n^{v}(\mathbf{k})$ can be written as

$$\mathbf{\Omega}_n^{v}(\mathbf{k}) = \nabla_{\mathbf{k}} \times \boldsymbol{\mathcal{A}}_n^{v}(\mathbf{k}) = -i\,\mathbf{v}_n \times \nabla_{\mathbf{k}} \left(\bar{C}_n^{\dagger}\, \bar{\bar{\Delta}}\, \bar{C}_n \right) \tag{5.43}$$

$$= -i\,\mathbf{v}_n \times \Big(\nabla_{\mathbf{k}}\, \bar{C}_n^{\dagger}\, \bar{\bar{\Delta}}\, \bar{C}_n + \underbrace{\bar{C}_n^{\dagger}\, \nabla_{\mathbf{k}} \bar{\bar{\Delta}}\, \bar{C}_n}_{\mathbf{v}_n \times \nabla_{\mathbf{k}} \bar{\bar{\Delta}} = 0} + \bar{C}_n^{\dagger}\, \bar{\bar{\Delta}}\, \nabla_{\mathbf{k}} \bar{C}_n \Big), \tag{5.44}$$

resulting to the expression

$$\mathbf{\Omega}_n^{v}(\mathbf{k}) = -i\,\mathbf{v}_n \times \Big[\Big(\bar{C}_n^{\dagger}\, \bar{\bar{\Delta}}^{\dagger}\, \nabla_{\mathbf{k}} \bar{C}_n \Big)^* + \bar{C}_n^{\dagger}\, \bar{\bar{\Delta}}\, \nabla_{\mathbf{k}} \bar{C}_n \Big]. \tag{5.45}$$

Finally, the component $\mathbf{\Omega}_n^r(\mathbf{k})$ is calculated as

$$\mathbf{\Omega}_n^r(\mathbf{k}) = \nabla_\mathbf{k} \times \boldsymbol{\mathcal{A}}_n^r(\mathbf{k}) = \nabla_\mathbf{k} \times \left(\bar{C}_n^\dagger \,\bar{\bar{\mathbf{r}}}\, \bar{C}_n\right) \tag{5.46}$$

$$= \sum_{\Lambda,\Lambda'} \int \nabla_\mathbf{k} \left(C_\Lambda^{n*}\, R_\Lambda^\dagger\, R_{\Lambda'}\, C_{\Lambda'}^n\right) \times \mathbf{r}\, d\mathbf{r} + \underbrace{\sum_{\Lambda,\Lambda'} \int C_\Lambda^{n*}\, R_\Lambda^\dagger\, R_{\Lambda'}\, C_{\Lambda'}^n \times \nabla_\mathbf{k}\mathbf{r}\, d\mathbf{r}}_{\nabla_\mathbf{k}\mathbf{r}=0} \tag{5.47}$$

$$= 2 \cdot \mathrm{Re}\left\{ \sum_{\Lambda,\Lambda'} \int \left[C_\Lambda^{n*}\, R_\Lambda^\dagger\, \nabla_\mathbf{k} \left(C_{\Lambda'}^n\, R_{\Lambda'}\right)\right] \times \mathbf{r}\, d\mathbf{r} \right\} \tag{5.48}$$

$$= 2 \cdot \mathrm{Re}\left\{ \sum_{\Lambda,\Lambda'} \int \left[\mathbf{v}_n \times C_\Lambda^{n*}\, R_\Lambda^\dagger\, \mathbf{r}\, \frac{\partial R_{\Lambda'}}{\partial E}\, C_{\Lambda'}^n\right] d\mathbf{r} \right\} \tag{5.49}$$

$$- 2 \cdot \mathrm{Re}\left\{ \sum_{\Lambda,\Lambda'} \int \left[C_\Lambda^{n*}\, R_\Lambda^\dagger\, \mathbf{r}\, R_{\Lambda'} \times \nabla_\mathbf{k} C_{\Lambda'}^n\right] d\mathbf{r} \right\} \tag{5.50}$$

$$= 2 \cdot \mathbf{v}_n \times \mathrm{Re}\left\{ \bar{C}_n^\dagger\, \bar{\bar{\mathbf{r}}}_E\, \bar{C}_n \right\} - 2 \cdot \mathrm{Re}\left\{ \bar{C}_n^\dagger\, \bar{\bar{\mathbf{r}}} \times \nabla_\mathbf{k} \bar{C}_n \right\}, \tag{5.51}$$

with

$$(\bar{\bar{\mathbf{r}}}_E)_{\Lambda,\Lambda'}(E) = \int_\omega R_\Lambda^\dagger(E;\mathbf{r})\, \mathbf{r}\, \frac{\partial R_{\Lambda'}(E;\mathbf{r})}{\partial E} d\mathbf{r}. \tag{5.52}$$

The final form is obtained by inserting the completeness relation (5.33)

$$\mathbf{\Omega}_n^r(\mathbf{k}) = 2 \cdot \mathbf{v}_n \times \mathrm{Re}\left\{ \bar{C}_n^\dagger\, \bar{\bar{\mathbf{r}}}_E\, \bar{C}_n \right\} - 2 \cdot \mathrm{Re}\left\{ \sum_m \frac{\bar{C}_n^\dagger\, \bar{\bar{\mathbf{r}}}\, \bar{C}_m \times \bar{D}_m^\dagger\, \nabla_\mathbf{k} \bar{C}_n}{\bar{D}_m^\dagger\, \bar{C}_m} \right\}. \tag{5.53}$$

In summary, the Abelian Berry curvature of the Bloch states can be calculated from (5.32), where its components are given by (5.42), (5.45) and (5.53) respectively. For this purpose, the right $\bar{C}$ and left $\bar{D}$ eigenvectors of the KKR matrix are needed, together with the group velocity $\mathbf{v}_n$ and the matrices $\bar{\bar{\rho}}, \bar{\bar{\Delta}}, \bar{\bar{\mathbf{r}}}$ and $\bar{\bar{\mathbf{r}}}_E$. It must be made clear that the eigenvectors which enter the KKR expansion (5.1) and the relations (5.42), (5.45) and (5.53) are correctly normalized in the way that is described in Subsection 3.3.3. On the contrary, the eigenvectors which enter the group velocity expression (5.13) are the ones that are obtained directly from the numerical subroutine that performs the KKR matrix diagonalization and have euclidean norm 1. Furthermore, the way that the total derivative $\nabla_\mathbf{k}\bar{C}_n$ is calculated will be analyzed in Section 5.4, while the representation of the matrices $\bar{\bar{\rho}}, \bar{\bar{\Delta}}, \bar{\bar{\mathbf{r}}}$ and $\bar{\bar{\mathbf{r}}}_E$ in the KKR framework will be analyzed in Section 5.5. In practice, the above calculations are performed at specified energy. The Green function, the t-matrix and the above matrices are calculated once per energy. Then, the shape of the constant energy surface which corresponds to the lattice BZ is determined. For every $\mathbf{k}$-point in this surface the KKR matrix is calculated, resulting in the group velocity and, finally, the Berry curvature of the Bloch bands is obtained.

5.4 Total derivative of KKR eigenvectors

In Subsection 3.3.3 the correct normalization of the eigenvectors of the KKR matrix was introduced as

$$\bar{C}_n = \frac{\bar{\bar{C}}_n}{\sqrt{P}}, \quad \text{with} \quad P = \bar{\bar{C}}_n^{\dagger}\, \bar{\bar{\rho}}\, \bar{\bar{C}}_n. \tag{5.54}$$

Both the eigenvectors and the norm P of the wavefunction depend on the wavevector $\mathbf{k}$ and the band energy $E_n(\mathbf{k})$. Thus, the total derivative is given by

$$\nabla_{\mathbf{k}} \bar{C}_n = \nabla_{\mathbf{k}} \left(\frac{\bar{\bar{C}}_n}{\sqrt{P}} \right) = \frac{\sqrt{P}\, \nabla_{\mathbf{k}} \bar{\bar{C}}_n - \bar{\bar{C}}_n\, \nabla_{\mathbf{k}} \sqrt{P}}{\left(\sqrt{P}\right)^2} = \frac{\nabla_{\mathbf{k}} \bar{\bar{C}}_n}{\sqrt{P}} - \frac{\bar{\bar{C}}_n\, \nabla_{\mathbf{k}} P}{2\left(\sqrt{P}\right)^3}, \tag{5.55}$$

where

$$\nabla_{\mathbf{k}} \sqrt{P} = \frac{\nabla_{\mathbf{k}} P}{2\sqrt{P}}. \tag{5.56}$$

The total derivative $\nabla_{\mathbf{k}} P$ is calculated as

$$\begin{aligned}
\nabla_{\mathbf{k}} P &= \nabla_{\mathbf{k}} \left(\bar{\bar{C}}_n^{\dagger}\, \bar{\bar{\rho}}\, \bar{\bar{C}}_n \right) && (5.57)\\
&= \nabla_{\mathbf{k}} \bar{\bar{C}}_n^{\dagger}\, \bar{\bar{\rho}}\, \bar{\bar{C}}_n + \bar{\bar{C}}_n^{\dagger}\, \nabla_{\mathbf{k}} \bar{\bar{\rho}}\, \bar{\bar{C}}_n + \bar{\bar{C}}_n^{\dagger}\, \bar{\bar{\rho}}\, \nabla_{\mathbf{k}} \bar{\bar{C}}_n && (5.58)\\
&= \left(\bar{\bar{C}}_n^{\dagger}\, \bar{\bar{\rho}}\, \nabla_{\mathbf{k}} \bar{\bar{C}}_n \right)^{*} + \bar{\bar{C}}_n^{\dagger} \left(\mathbf{v}_n \bar{\bar{\Delta}}^{\dagger} + \mathbf{v}_n \bar{\bar{\Delta}} \right) \bar{\bar{C}}_n + \bar{\bar{C}}_n^{\dagger}\, \bar{\bar{\rho}}\, \nabla_{\mathbf{k}} \bar{\bar{C}}_n && (5.59)\\
&= 2 \cdot \mathrm{Re}\left\{ \bar{\bar{C}}_n^{\dagger}\, \bar{\bar{\rho}}\, \nabla_{\mathbf{k}} \bar{\bar{C}}_n \right\} + 2 \cdot \mathbf{v}_n \cdot \mathrm{Re}\left\{ \bar{\bar{C}}_n^{\dagger}\, \bar{\bar{\Delta}}\, \bar{\bar{C}}_n \right\}. && (5.60)
\end{aligned}$$

The total derivative $\nabla_{\mathbf{k}} \bar{\bar{C}}_n$ is calculated numerically as

$$\begin{aligned}
\nabla_{\mathbf{k}} \bar{\bar{C}}_n(\mathbf{k}) &= \left. \frac{\partial \bar{\bar{C}}_n}{\partial \mathbf{k}} \right|_{E=E_n(\mathbf{k})} + \mathbf{v}_n \left. \frac{\partial \bar{\bar{C}}_n}{\partial E} \right|_{E=E_n(\mathbf{k})} && (5.61)\\
&= \frac{1}{2\,\delta \mathbf{k}} \Big[\bar{\bar{C}}_n(\mathbf{k} + \delta\mathbf{k}, E_n(\mathbf{k})) - \bar{\bar{C}}_n(\mathbf{k} - \delta\mathbf{k}, E_n(\mathbf{k})) \Big] && (5.62)\\
&\quad + \mathbf{v}_n \frac{1}{2\,\delta E} \Big[\bar{\bar{C}}_n(\mathbf{k}, E_n(\mathbf{k}) + \delta E) - \bar{\bar{C}}_n(\mathbf{k}, E_n(\mathbf{k}) - \delta E) \Big]. && (5.63)
\end{aligned}$$

5.5 KKR representation of matrices

The matrices $\bar{\bar{\rho}}$, $\bar{\bar{\Delta}}$ and the vector matrices $\bar{\bar{\mathbf{r}}}$, $\bar{\bar{\mathbf{r}}}_E$, which appear in the relations for the Berry curvature, contain an integration over the unit cell ω which is treated explicitly in the KKR framework. As seen in Subsection 3.3.3, the shape functions $\Theta(\mathbf{r})$ enter in the integration and they are expanded, together with the regular wavefunctions $R(\mathbf{r}, E)$, into real spherical harmonics.

An expression for the $\bar{\bar{\rho}}$ matrix has already been obtained (3.44), (3.48). For only one atom in the unit cell it yields

$$(\bar{\bar{\rho}})_{\Lambda,\Lambda'}(E) = \sum_{L_1,L_2,L_3} \mathcal{C}_{L_1,L_2,L_3} \int dr \sum_{\sigma} \left[R^{\sigma}_{L_1\Lambda}(r;E)\right]^* R^{\sigma}_{L_2\Lambda'}(r;E)\, \Theta_{L_3}(r), \quad (5.64)$$

and for the spherically symmetric contribution $\left(L_3 = 0, \mathcal{C}_{L_1,L_2,0} = \frac{1}{\sqrt{4\pi}}\delta_{L_1,L_2}, \Theta_0(\mathbf{r}) = \sqrt{4\pi}\right)$

$$(\bar{\bar{\rho}})^{sph}_{\Lambda,\Lambda'}(E) = \sum_{L_1} \frac{1}{\sqrt{4\pi}} \int dr \sum_{\sigma} \left[R^{\sigma}_{L_1\Lambda}(r;E)\right]^* R^{\sigma}_{L_1\Lambda'}(r;E)\, \Theta_0(r). \quad (5.65)$$

In the same way, the matrix $\bar{\bar{\Delta}}$ is calculated as

$$\left(\bar{\bar{\Delta}}\right)_{\Lambda,\Lambda'}(E) = \sum_{L_1,L_2,L_3} \mathcal{C}_{L_1,L_2,L_3} \int dr \sum_{\sigma} \left[R^{\sigma}_{L_1\Lambda}(r;E)\right]^* \frac{\partial R^{\sigma}_{L_2\Lambda'}(r;E)}{\partial E}\, \Theta_{L_3}(r), \quad (5.66)$$

while the spherically symmetric contribution is

$$\left(\bar{\bar{\Delta}}\right)^{sph}_{\Lambda,\Lambda'}(E) = \sum_{L_1} \frac{1}{\sqrt{4\pi}} \int dr \sum_{\sigma} \left[R^{\sigma}_{L_1\Lambda}(r;E)\right]^* \frac{\partial R^{\sigma}_{L_1\Lambda'}(r;E)}{\partial E}\, \Theta_0(r). \quad (5.67)$$

The vector matrices $\bar{\bar{\mathbf{r}}}$ and $\bar{\bar{\mathbf{r}}}_E$ are treated in a different way because of the presence of the vector $\mathbf{r}$ in the integration, which is also expanded into real spherical harmonics as

$$\mathbf{r} = \sum_{L} \mathbf{f}_L(r) Y_L(\hat{r}). \quad (5.68)$$

That yields an additional spherical harmonic, so the integration of four spherical harmonics has to be performed. A detailed derivation is shown below for the vector matrix $\bar{\bar{\mathbf{r}}}$.

Starting from the expansion into real spherical harmonics one obtains

$$(\bar{\bar{\mathbf{r}}})_{\Lambda,\Lambda'}(E) = \int_{\omega} R^{\dagger}_{\Lambda}(E;\mathbf{r})\, \mathbf{r}\, R_{\Lambda'}(E;\mathbf{r})\, d\mathbf{r} \quad (5.69)$$

$$= \sum_{L_1,L_2,L_3,L_4} \int dr \sum_{\sigma} \left[R^{\sigma}_{L_1\Lambda}(r;E)\right]^* R^{\sigma}_{L_2\Lambda'}(r;E)\, \Theta_{L_3}(r)\, \mathbf{f}_{L_4}(r) \quad (5.70)$$

$$\cdot \int Y_{L_1}(\hat{r})\, Y_{L_2}(\hat{r})\, Y_{L_3}(\hat{r})\, Y_{L_4}(\hat{r})\, d\Omega. \quad (5.71)$$

In order to perform the integral of the four spherical harmonics, the idea described in Appendix A of [49] is followed. At first, two spherical harmonics are expressed as a linear combination of a single spherical harmonic

$$Y_{L_3}(\hat{r})\, Y_{L_4}(\hat{r}) = \sum_L c_L(L_3, L_4)\, Y_L(\hat{r}), \tag{5.72}$$

where the coefficients $c_L(L_3, L_4)$ are given by

$$c_L(L_3, L_4) = \int Y_{L_3}(\hat{r})\, Y_{L_4}(\hat{r})\, Y_L^*(\hat{r})\, d\Omega = \int Y_{L_3}(\hat{r})\, Y_{L_4}(\hat{r})\, Y_L(\hat{r})\, d\Omega = \mathcal{C}_{L_3,L_4,L}, \tag{5.73}$$

because for the real spherical harmonics holds $Y_L^* = Y_L$. Thus, the integral of four spherical harmonics can be written as

$$\int Y_{L_1}(\hat{r})\, Y_{L_2}(\hat{r})\, Y_{L_3}(\hat{r})\, Y_{L_4}(\hat{r})\, d\Omega = \sum_L \int Y_{L_1}(\hat{r})\, Y_{L_2}(\hat{r})\, Y_L(\hat{r})\, \mathcal{C}_{L_3,L_4,L}\, d\Omega \tag{5.74}$$

$$= \sum_L \mathcal{C}_{L_1,L_2,L}\, \mathcal{C}_{L_3,L_4,L} \tag{5.75}$$

The property of the Gaunt coefficients [15]

$$\mathcal{C}_{L,L',L''} \neq 0 \quad \text{only if} \quad |l' - l''| \leq l \leq l' + l'' \quad \text{and} \quad m = m' + m'', \tag{5.76}$$

restricts the dummy index $L = (l, m)$ in the range

$$|l_{1(3)} - l_{2(4)}| \leq l \leq l_{1(3)} + l_{2(4)} \quad \text{with} \quad m = m_{1(3)} + m_{2(4)}. \tag{5.77}$$

Therefore, the $\bar{\bar{\mathbf{r}}}$ vector matrix is calculated from the relation

$$(\bar{\bar{\mathbf{r}}})_{\Lambda,\Lambda'}(E) = \sum_{\substack{L_1,L_2,L_3,\\ L_4,L,\sigma}} \mathcal{C}_{L_1,L_2,L}\mathcal{C}_{L_3,L_4,L} \int dr \left[R^\sigma_{L_1\Lambda}(r;E)\right]^* R^\sigma_{L_2\Lambda'}(r;E)\Theta_{L_3}(r)\mathbf{f}_{L_4}(r), \tag{5.78}$$

$$\text{where} \quad \mathbf{f}_{L_4}(r) = r\sqrt{\frac{4\pi}{3}}\,\hat{r}, \quad \text{and} \quad L_4 = 2, 3, 4. \tag{5.79}$$

The resulting expression for the vector function $\mathbf{f}_{L_4}(r)$ is obtained by an analytic calculation in the spherical coordinate system. Also, the spherically symmetric contribution is

$$(\bar{\bar{\mathbf{r}}})^{sph}_{\Lambda,\Lambda'}(E) = \sum_{L_1,L_2,L_4,\sigma} \mathcal{C}_{L_1,L_2,L_4} \frac{1}{\sqrt{4\pi}} \int dr\, \left[R^\sigma_{L_1\Lambda}(r;E)\right]^* R^\sigma_{L_2\Lambda'}(r;E)\, \Theta_0(r)\, \mathbf{f}_{L_4}(r). \tag{5.80}$$

With the same procedure the vector matrix $\bar{\bar{\mathbf{r}}}_E$ is calculated from the relations

$$(\bar{\bar{\mathbf{r}}}_E)_{\Lambda,\Lambda'}(E) = \sum_{\substack{L_1,L_2,L_3,\\ L_4,L,\sigma}} \mathcal{C}_{L_1,L_2,L}\mathcal{C}_{L_3,L_4,L} \int dr \left[R^{\sigma}_{L_1\Lambda}(r;E)\right]^* \frac{\partial R^{\sigma}_{L_2\Lambda'}(r;E)}{\partial E} \Theta_{L_3}(r)\mathbf{f}_{L_4}(r) \tag{5.81}$$

and

$$(\bar{\bar{\mathbf{r}}}_E)^{sph}_{\Lambda,\Lambda'}(E) = \sum_{L_1,L_2,L_4,\sigma} \mathcal{C}_{L_1,L_2,L_4} \frac{1}{\sqrt{4\pi}} \int dr \left[R^{\sigma}_{L_1\Lambda}(r;E)\right]^* \frac{\partial R^{\sigma}_{L_2\Lambda'}(r;E)}{\partial E} \Theta_0(r)\, \mathbf{f}_{L_4}(r). \tag{5.82}$$

5.6 Application in AHE

The Berry curvature calculated from (5.32) is used to determine the intrinsic AHC. For a ferromagnetic system with magnetization **M** along the z axis, only the z component $\Omega_z(\mathbf{k}) = \sum_n \Omega^z_n(\mathbf{k}) \neq 0$, due to the symmetry restrictions seen in Appendix A. Then, the expression for the transverse AHC is given by (4.38) as

$$\sigma^c_{xy} = -\frac{e^2}{\hbar(2\pi)^3} \sum_n \int_{BZ} d\mathbf{k}\, f_{n\mathbf{k}}\, \Omega^z_n(\mathbf{k}). \tag{5.83}$$

The last relation is further written as

$$\sigma^c_{xy} = -\frac{e^2}{\hbar(2\pi)^3} \int^{E_F} d\mathcal{E}\, \Omega^z(\mathcal{E}), \tag{5.84}$$

where the energy resolved Berry curvature is introduced as

$$\Omega^z(\mathcal{E}) = \sum_n \int_{IS(E)} \frac{d^2\, k}{\mid \mathbf{v}^n_F(\mathbf{k}) \mid} \Omega^z_n(\mathbf{k}). \tag{5.85}$$

The isosurface (IS) integral is performed for a dense integration mesh of energies up to the Fermi energy level $E = E_F$. Then, by artificially shifting the Fermi energy, the intrinsic AHC (5.84) is calculated as a function of E_F.

Chapter 6

Berry curvature and anomalous Hall conductivity (AHC) calculations for the ferromagnetic bcc Fe

In this thesis, the studied system is ferromagnetic bcc Fe, with magnetization **M** along the z-axis. The calculations were carried out by using the Jülich KKR code [50]. The self-consistent calculation of the potential together with the calculations for the Green function and the t-matrix were computed with the *KKRhost* program. The Fermi formalism of the Berry curvature was implemented in the *PKKprime* code, which previously included the Fermi surface and Bloch wavefunction calculation.

The self-consistent calculations for the potential were performed for two different l_{max} cutoffs and for a lattice constant $a = 5.4$a.u[1]. For $l_{\text{max}} = 3$, the total magnetic moment in the unit cell was $2.18\mu_{\text{B}}$. Also, for $l_{\text{max}} = 2$, the total magnetic moment in the unit cell was $2.23\mu_{\text{B}}$.

6.1 Berry curvature

In the first step, the Berry curvature, given from (5.32), can be calculated over the Fermi surface. The calculations are performed for $l_{\text{max}} = 3$, $l_{\text{max}} = 2$ and $l_{\text{max}} = 2$ with increased spin-orbit coupling strength $\xi = 2$, instead of $\xi = 1$ (3.51). The results for the absolute value of the Berry curvature on the Fermi surface are represented in Fig.(6.1). In order to find the Fermi surface, an initial $12 \times 12 \times 12$ k-points grid is chosen, which after further refinements results to a mesh of $96 \times 96 \times 96$ k-points. This grid size is sufficient to resolve the small Fermi surface branches of bcc Fe, but, as is it will be shown afterwards, it is not fine enough to accurately calculate the value of the Berry curvature.

[1] a.u. denotes atomic Rydberg units. 1a.u.=0.529Å

Thus, Fig.(6.1) can only be used to have a qualitative image of the behavior of the Berry curvature.

The first observation one can make is that the value of $|\mathbf{\Omega}_n(\mathbf{k})|$ is almost everywhere close to zero, except from small regions where its value is very large. In these regions, also called "hot-spots", avoided crossings of two bands appear, due to the spin-orbit coupling interaction, leading to the rise of the Berry curvature. They are mostly located near the points where the Fermi surface touches the BZ boundaries, or, near the points where different energy bands of the Fermi surface come close. Furthermore, the angular momentum cutoff ($l_{\max} = 2$ or 3) affects the calculations and results to a slightly different Fermi surface shape and, also, to higher values for the Berry curvature for $l_{\max} = 2$. Last but not least, as expected, the increase in the spin-orbit coupling strength results to a decrease in the Berry curvature.

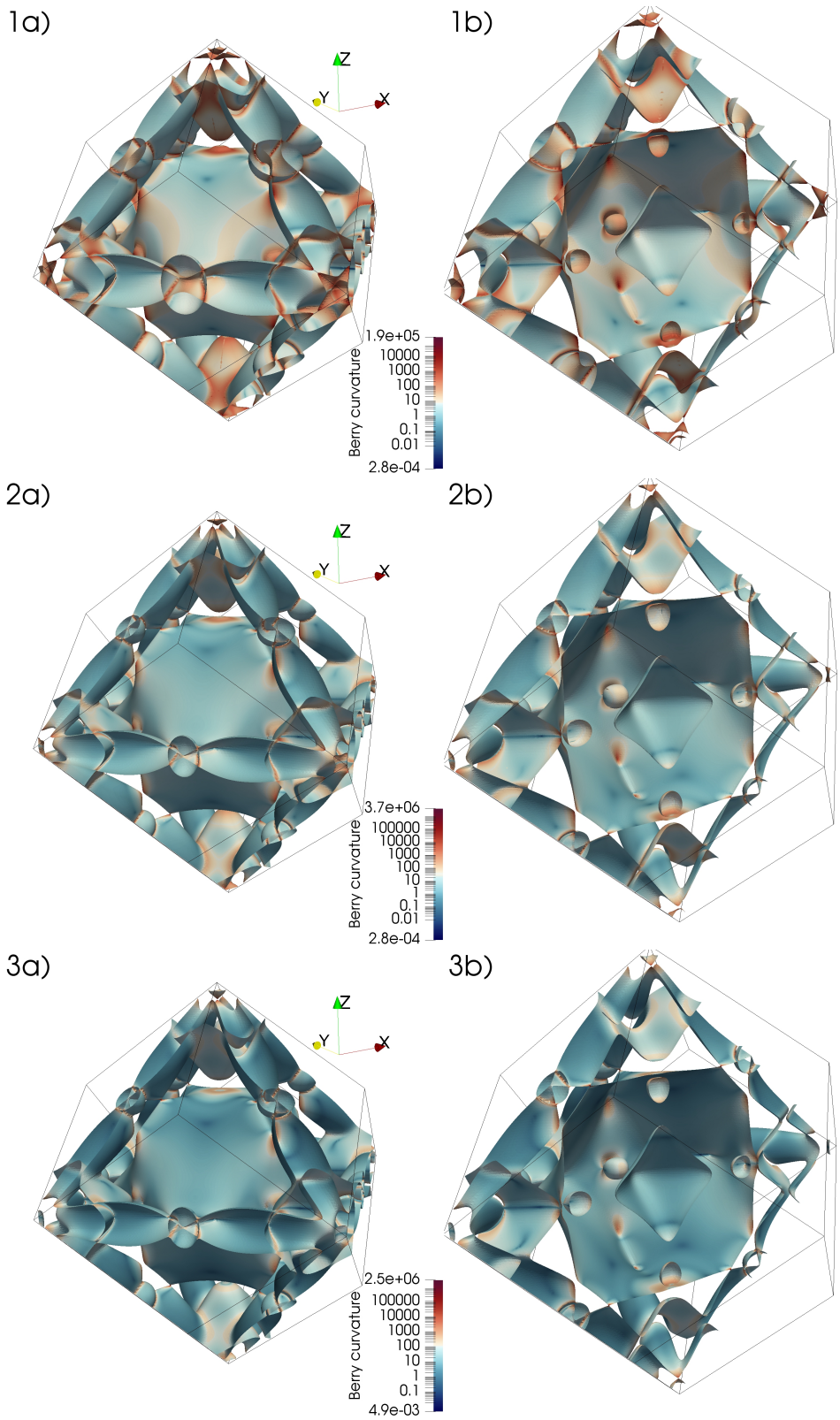

Figure 6.1: *The absolute value of the Berry curvature* $|\mathbf{\Omega}_n(\mathbf{k})|$*, in atomic Rydberg units, on the Fermi surface of the ferromagnetic bcc Fe for (1)* $l_{\max} = 3$*, (2)* $l_{\max} = 2$ *and (3)* $l_{\max} = 2$ *with increased spin-orbit coupling strength* $\xi = 2$*. In (1a),(2a) and (3a) the whole Fermi surface is depicted, whereas in (1b), (2b) and (3b), only the half Fermi surface is represented in order to demonstrate nested branches of the Fermi surface.*

6.2 Energy resolved Berry curvature

In this part, the energy resolved Berry curvature $\Omega^z(\mathcal{E})$ is calculated from (5.85). In order to do this, the sufficient size of the k-points grid has to be decided first. By increasing the grid size, the value where $\Omega^z(\mathcal{E})$ converges is sought for, together with the condition that $\Omega^x(\mathcal{E}) = \Omega^y(\mathcal{E}) = 0$. For $l_{\max} = 3$, starting from a $12 \times 12 \times 12$ k-points grid and up until a $22 \times 22 \times 22$ grid, the convergence is not met. The need for more refined and more time-demanding surface mapping can be covered with the much faster $l_{\max} = 2$ choice. In that case, one deals with KKR matrices of a 18×18 dimension, instead of a 32×32 dimension for $l_{\max} = 3$. Therefore, for $l_{\max} = 2$, convergence is met at a $28 \times 28 \times 28$ grid. The convergence process can be seen in Table 6.1 for $l_{\max} = 3$ and in Table 6.2 for $l_{\max} = 2$. For the rest of the calculations within this thesis, the $26 \times 26 \times 26$ k-points grid is chosen.

$l_{\max} = 3$			
k-points grid size	$\Omega^x(\mathcal{E})$	$\Omega^y(\mathcal{E})$	$\Omega^z(\mathcal{E})$
12×12×12	-1.00E+00	8.44E-01	-2.94E+02
14×14×14	2.17E-02	4.05E-02	3.81E+01
16×16×16	-1.15E+00	2.11E-01	4.88E+02
18×18×18	9.91E-01	1.24E+00	4.27E+02
20×20×20	-5.11E+01	8.89E+01	2.42E+02
22×22×22	-3.23E+01	9.12E+00	4.04E+02

Table 6.1: *Convergence process for the decision of the k-points grid size for $l_{\max} = 3$.*

$l_{\max} = 2$			
k-points grid size	$\Omega^x(\mathcal{E})$	$\Omega^y(\mathcal{E})$	$\Omega^z(\mathcal{E})$
12×12×12	-5.01E+00	9.31E+00	-4.33E+03
22×22×22	1.41E+01	8.66E+00	-2.18E+03
24×24×24	4.62E+00	9.73E+00	-1.52E+03
26×26×26	1.36E+01	5.79E+00	-1.47E+03
28×28×28	4.74E+01	-8.72E+00	-1.37E+03

Table 6.2: *Convergence process for the decision of the k-points grid size for $l_{\max} = 2$.*

After deciding the suitable k-points grid size, $\Omega^z(\mathcal{E})$ is calculated in the energy interval $[E_F - 0.6\text{Ry}, E_F + 0.25\text{Ry}]$. The density of states (DOS) diagram of the ferromagnetic bcc Fe appears in Fig.(6.2). The sharp peaks come from the d electron states, whereas the rest, almost flat, contribution comes from the s and p electron states.

The first calculation of $\Omega^z(\mathcal{E})$ is performed for the $\xi = 1$ case (regular SOC strength). As stated in [4], the spiky character of $\mathbf{\Omega(k)}$ demands a very dense energy mesh. The en-

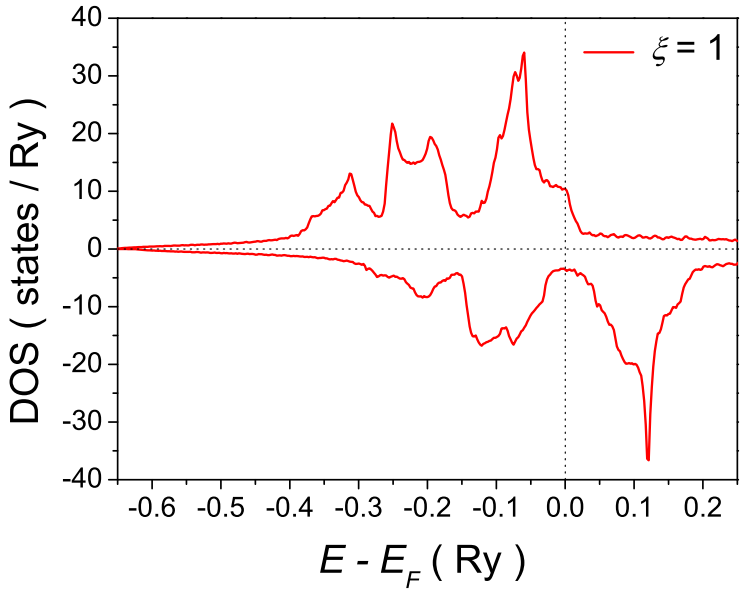

Figure 6.2: *Density of states of the ferromagnetic bcc Fe, relative to the Fermi energy level.*

ergy partition is initially picked at 4mRy and successively decreased to 2mRy and 1mRy. The results can be seen in Fig.(6.3). Although a spiky behavior of $\Omega^z(\mathcal{E})$ is formed already at the 4mRy partition, when moving to the 2mRy and 1mRy partitions new peaks appear, or others that had already appeared become sharper. It is evident that a finer energy division is needed. The partition is further decreased in 0.5mRy, 0.25mRy and 0.125mRy. The calculated $\Omega^z(\mathcal{E})$ is also presented in Fig.(6.3). In the states above the Fermi energy, the shape of $\Omega^z(\mathcal{E})$ is not changed, so, its value at this region is converged. However, in the regions between $(-0.27, -0.2)$mRy and $(-0.15, 0.05)$mRy, convergence is not met because new peaks still appear. By focusing only on these two regions, the energy partition is further reduced to 0.0625mRy, 0.03125mRy and 0.015625mRy. The results for the partitions 0.0625mRy and 0.03125mRy and separately for the 0.015625mRy partition, are shown in Fig.(6.4). Even at these very small partitions, new peaks still appear or become sharper, making it difficult to come to a conclusion about the shape of $\Omega^z(\mathcal{E})$. One solution could be to perform more calculations in these regions and, perhaps, going to a finer partition. This could not be accomplished due to restrictions in the available computational time. Even without these restrictions, the results would still be unreliable. Such small precision may introduce a numerical instability which stems from the way that the KKR matrix equation is solved in order to define the band structure. Consequently, for the $\xi = 1$ case, it is not feasible to calculate a trustworthy shape for $\Omega^z(\mathcal{E})$. One can attribute this difficulty to the nature of Fe as a material with weak SOC. That leads to smaller avoided band crossings, which result in larger Berry curvature locally at these avoided crossings.

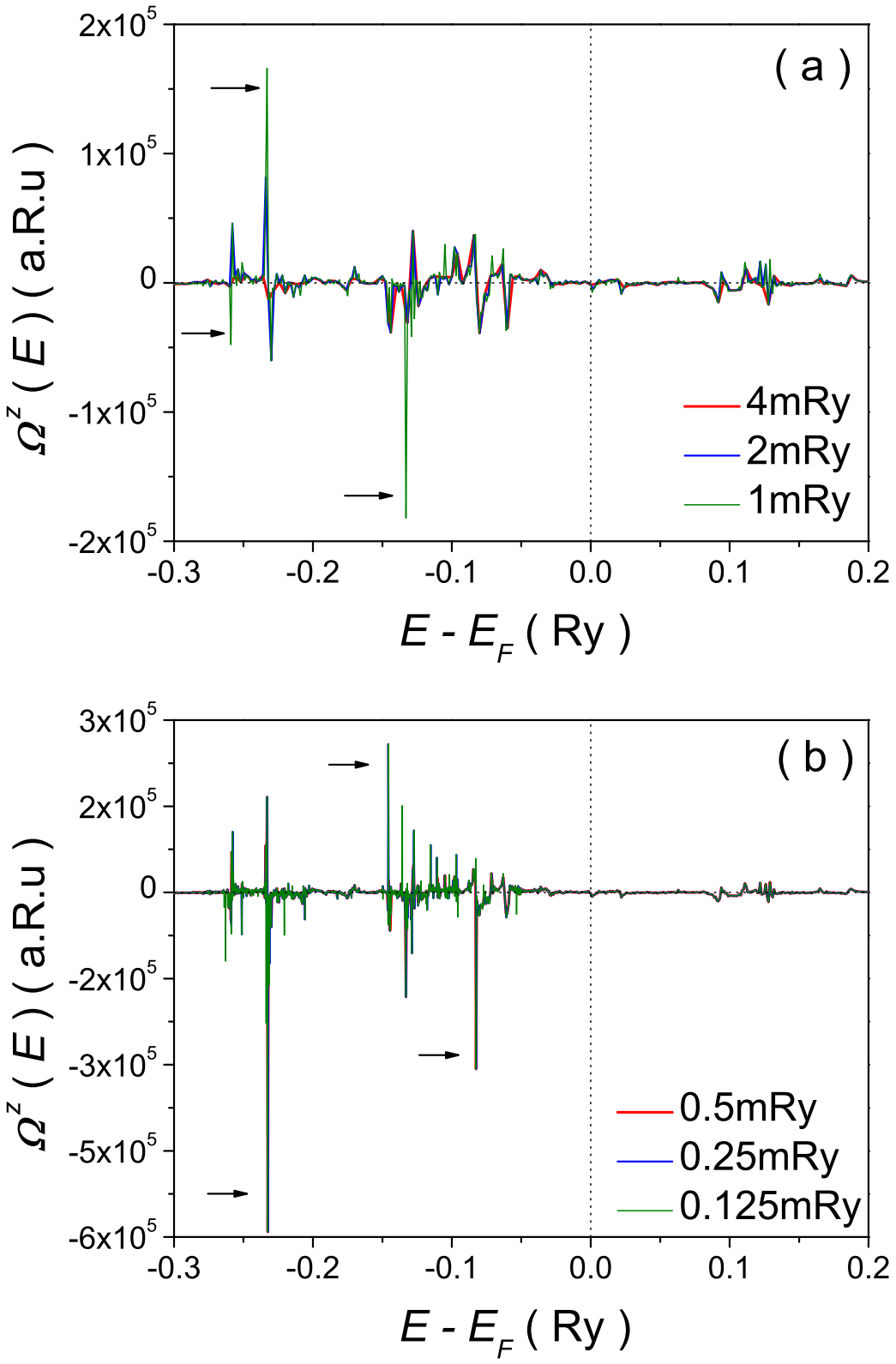

Figure 6.3: *Energy resolved Berry curvature $\Omega^z(\mathcal{E})$, in atomic Rydberg units (a.R.u), (a) for $4mRy$, $2mRy$ and $1mRy$ energy partitions and (b) for $0.5mRy$, $0.25mRy$ and $0.125mRy$ energy partitions. The results are presented relatively to the Fermi energy level. The arrows are used to indicate the new peaks that appear when the energy partition is decreased.*

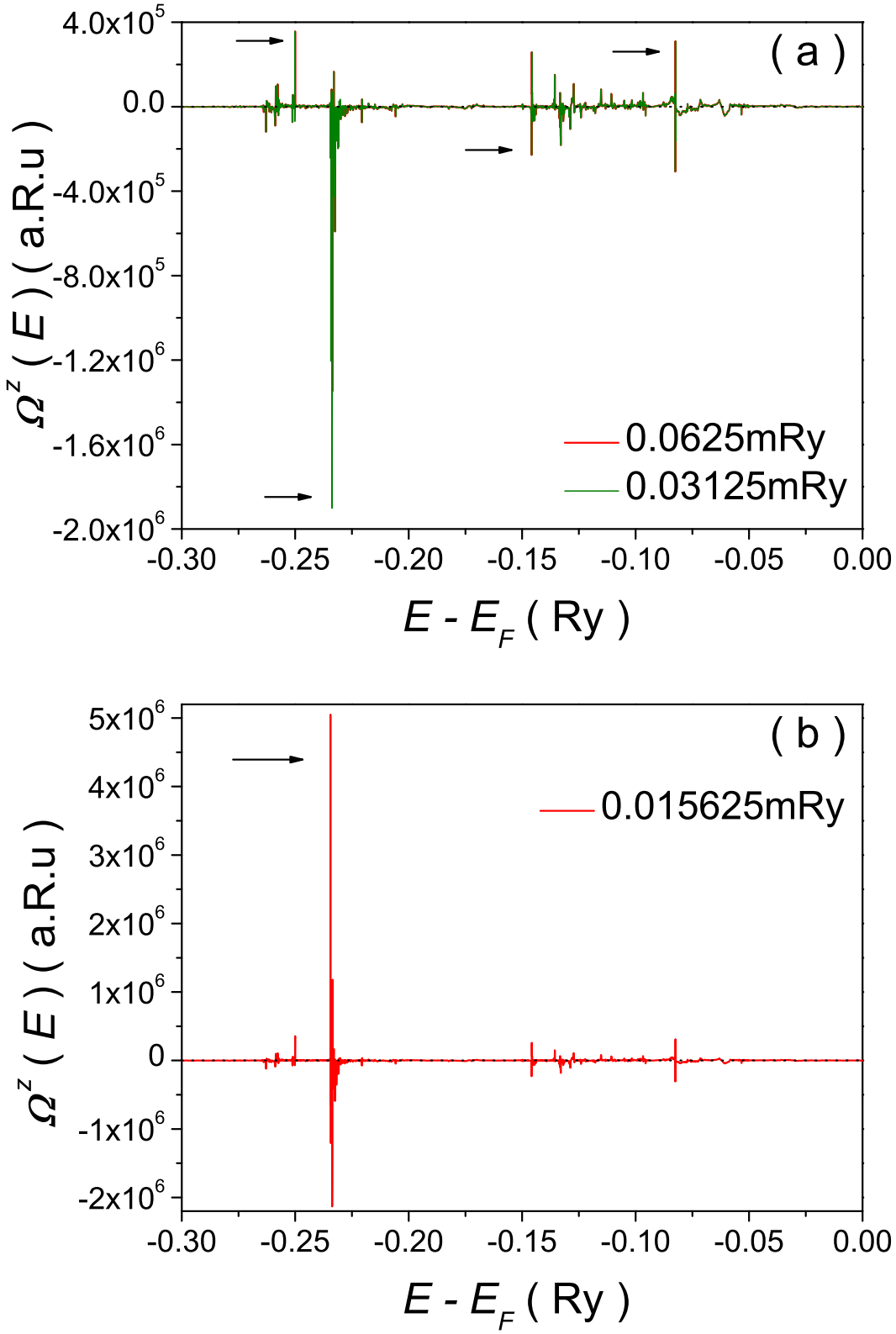

Figure 6.4: *Energy resolved Berry curvature $\Omega^z(\mathcal{E})$, in atomic Rydberg units (a.R.u), (a) for $0.0625mRy$ and $0.03125mRy$ energy partitions and (b) for $0.015625mRy$ energy partition. The results are presented relatively to the Fermi energy level. The arrows are used to indicate the new peaks that appear when the energy partition is decreased.*

In order to overcome the difficulty of needing a very dense energy mesh, the spin-orbit coupling strength is increased to $\xi = 2$. For this case, the energy partition of $0,05$mRy was found adequate. The calculated $\Omega^z(\mathcal{E})$, together with the corresponding DOS diagram, is presented in Fig.(6.5) for the $\xi = 2$ case. The spiky character of $\Omega^z(\mathcal{E})$ is well depicted, while the presentation together with the DOS diagram leads one to attribute the large contributions to $\Omega^z(\mathcal{E})$ to the d-electron peaks. In these regions the energy bands come close, so the Berry curvature is increased. In the states below 0.35Ry, where there are mostly s and p electron states, the Berry curvature vanishes. Also, in comparison with the $\xi = 1$ case, it can be seen that, the peaks of $\Omega^z(\mathcal{E})$ decrease with the increase in the spin-orbit coupling strength ξ. This is expected, because stronger SOC leads to larger splitting at avoided crossings (induced by SOC) and thus smaller values of $\Omega^z(\mathcal{E})$ at the peaks. It should be noticed that the splitting appears in the denominator of (2.20), causing the near divergence, while ξ appears in the numerator (included in the Hamiltonian), causing an overall smooth enhancement. In conclusion, this system seems more suitable for the calculation $\Omega^z(\mathcal{E})$, than the non-converging $\xi = 1$ case.

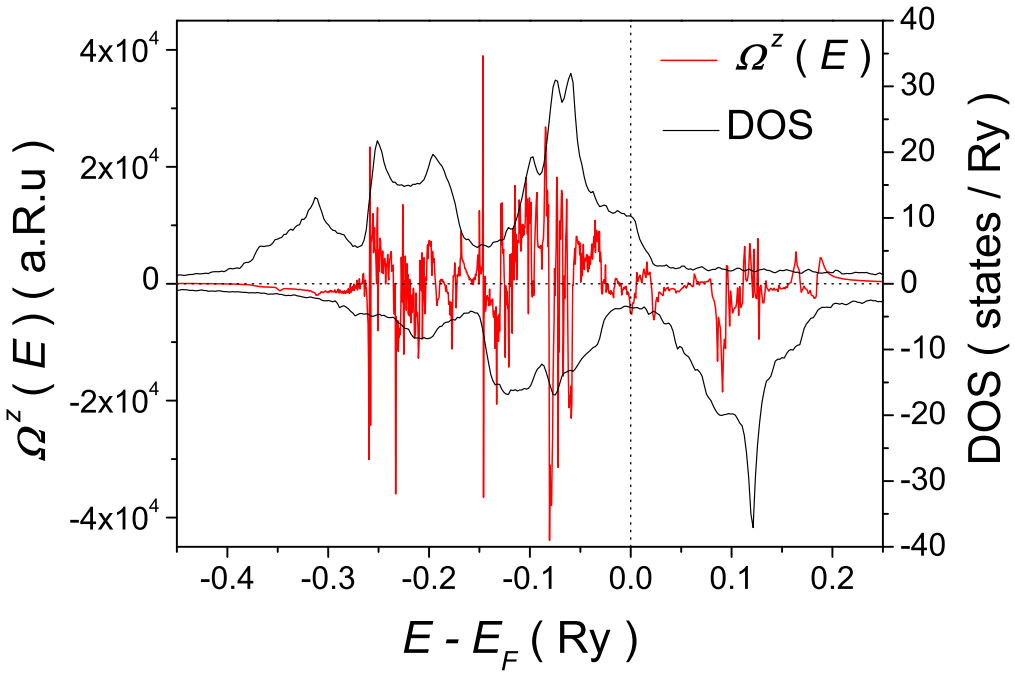

Figure 6.5: *Energy resolved Berry curvature $\Omega^z(\mathcal{E})$, in atomic Rydberg units (a.R.u), and density of states in the case of increased spin-orbit coupling strength $\xi = 2$. The results are presented relatively to the Fermi energy level.*

Next, the spin-orbit coupling strength is further increased to $\xi = 4$ and $\xi = 6$. The shape of the DOS diagram in relation to the different values of the strength ξ can be seen in Fig.(6.6). The effect of the increase in ξ is more significant in the region between

$(-0.15, 0)$Ry. The d-electron peaks formed in this region separate from each other and become sharper. For $\xi = 6$, these peaks have a totally different shape in comparison with the $\xi = 1$ case. $\Omega^z(\mathcal{E})$ is calculated for $\xi = 4$ with a 1mRy energy partition and for $\xi = 6$ with a 2mRy energy partition. The results are shown in Fig.(6.7), together with the $\xi = 2$ case. By further increasing ξ, the formed peaks are smoother and the overall shape becomes less spiky. This can be attributed to the further separation of the energy bands due to the increased spin-orbit interaction. Also, the value of $\Omega^z(\mathcal{E})$ does not decrease significantly, in comparison to the transition from $\xi = 1$ to $\xi = 2$. That maybe is because the overall smooth enhancement to the Berry curvature, caused by the increase in ξ, compensates for the further decrease, caused by the larger band splitting.

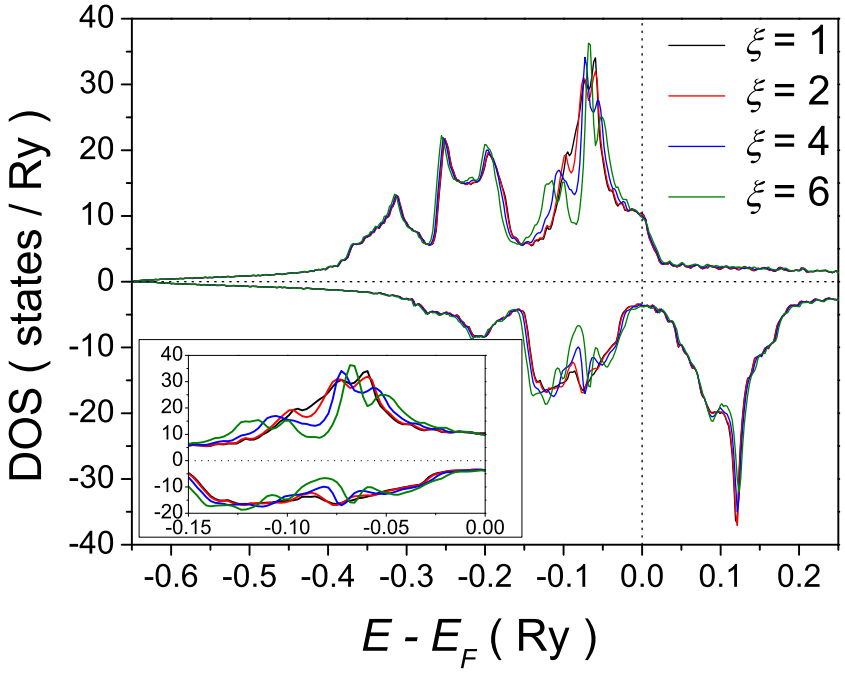

Figure 6.6: *Density of states of the ferromagnetic bcc Fe for different values of the spin-orbit coupling strength ξ. The results are presented relatively to the Fermi energy level.*

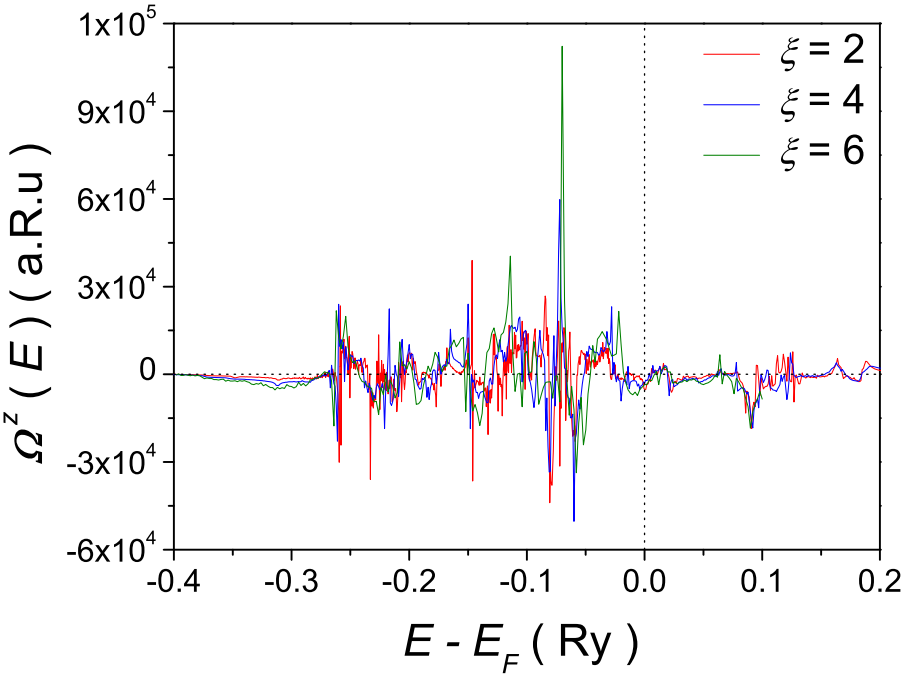

Figure 6.7: *Energy resolved Berry curvature $\Omega^z(\mathcal{E})$, in atomic Rydberg units (a.R.u), for different values of the spin-orbit coupling strength ξ. The results are presented relatively to the Fermi energy level.*

6.3 AHC calculation

After calculating the energy resolved Berry curvature, the intrinsic anomalous Hall conductivity $\sigma_{xy}(\mathcal{E})$ can be found from integrating the peaked function $\Omega^z(\mathcal{E})$ over the energies (see (5.84)), up to a final energy $\mathcal{E}$, i.e. $\sigma_{xy} = -\frac{e^2}{\hbar(2\pi)^3}\int^{\mathcal{E}} d\mathcal{E}'\ \Omega^z(\mathcal{E}')$. The physical value is at $\sigma_{xy}(\mathcal{E} = E_F)$. For the $\xi = 1$ case, the calculated σ_{xy} for some selected energy partitions can be seen in Fig.(6.8). It is clear that the convergence problem of this case is also present in σ_{xy}. From Fig.(6.8), it can be seen that the problematic regions are near $(-0.25, -0.2)$Ry and $(-0.15, -0.1)$Ry.

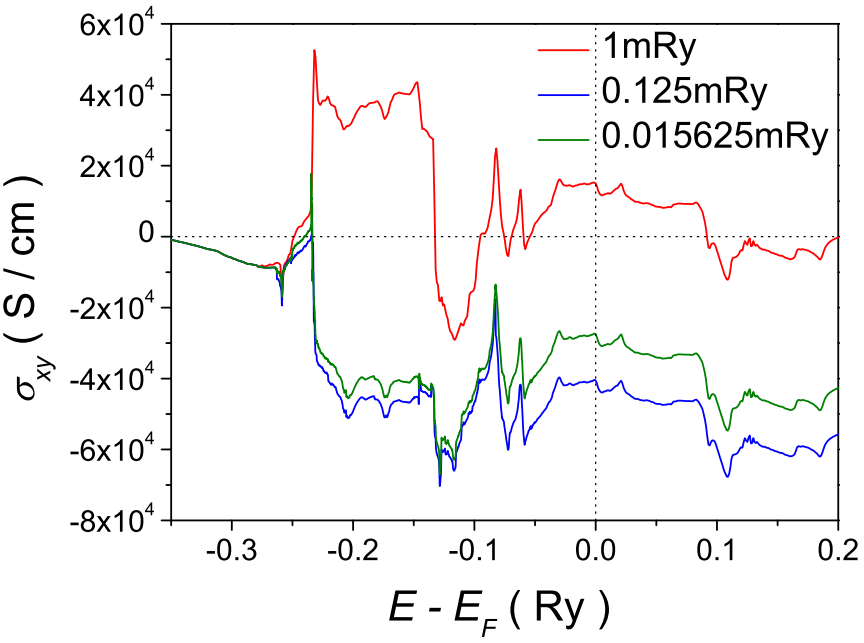

Figure 6.8: *Intrinsic anomalous Hall conductivity σ_{xy} for $1mRy$, $0.125mRy$ and $0.015625mRy$ energy partitions.The results are presented relatively to the Fermi energy level.*

Furthermore, σ_{xy} is also calculated for the cases where the spin-orbit coupling strength ξ is increased. The results are presented in Fig.(6.9). One can see how the increase in the spin-orbit coupling strength alters the shape of σ_{xy} in a smooth way. In Fig.(6.9) also the calculated σ_{xy} for $\xi = 1$ and 1mRy is included. It seems that this case approaches the ones where ξ is increased, while the differences are clearly located in the problematic regions near $(-0.25, -0.2)$Ry and $(-0.15, -0.1)$Ry. The behavior of σ_{xy} near the Fermi energy can be seen in Fig.(6.10). Although the shape of σ_{xy} calculated for $\xi = 1$ approaches the one calculated in [51], its value is approximately 20 times larger. Also, in Fig.(6.10) the calculated σ_{xy} at the Fermi energy can be seen in relation to the spin-orbit coupling strength ξ. Its shape is similar to the one obtained in [36], with the results

being again approximately 20 times larger. The origin of this discrepancy is not clear at present. For the $\xi = 1$ case, the calculated σ_{xy} for Fe, by other first-principles methods [36,37,40,51], ranges between 750S/cm and 800S/cm at zero temperature, while the experimentally measured value in room temperature is 1032S/cm [52].

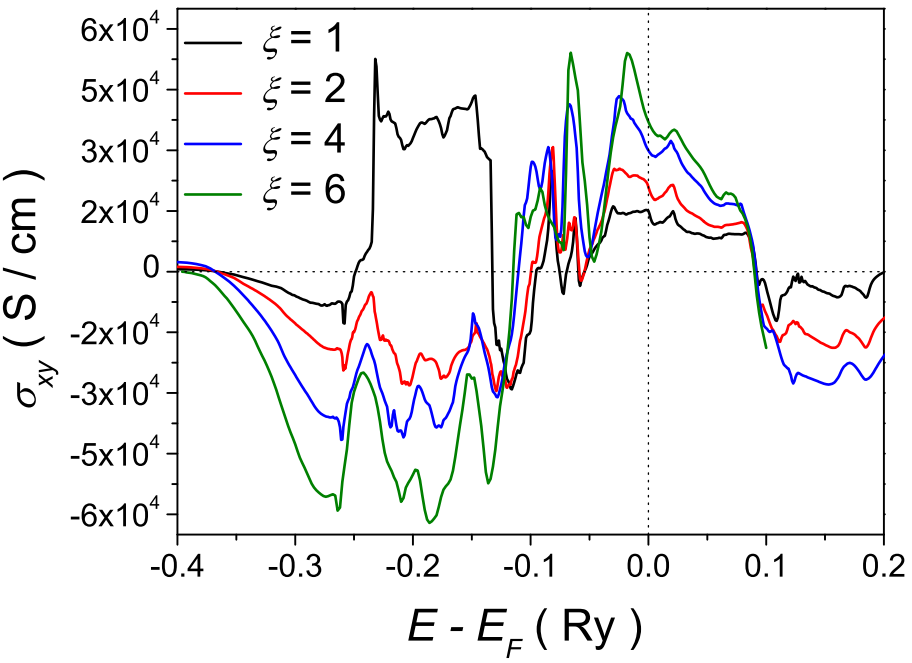

Figure 6.9: *Intrinsic anomalous Hall conductivity σ_{xy} for different values of the spin-orbit coupling strength ξ.The results are presented relatively to the Fermi energy level.*

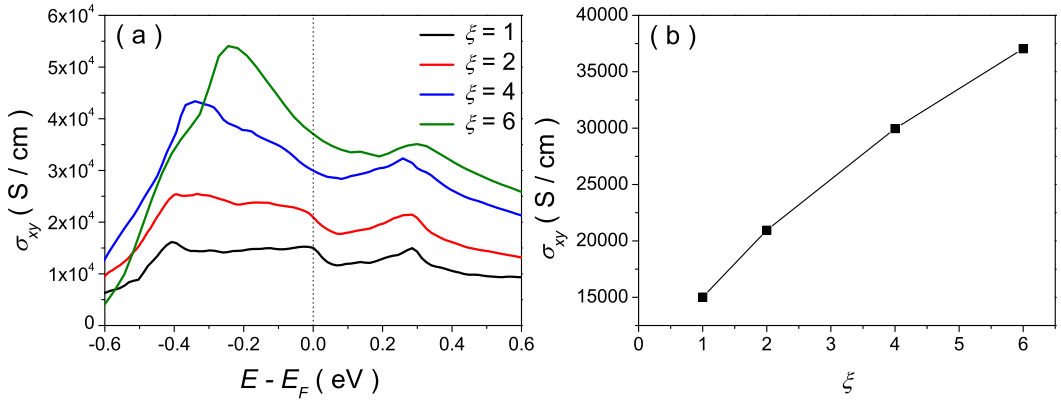

Figure 6.10: *(a) Intrinsic anomalous Hall conductivity σ_{xy}, around the Fermi energy, for different values of the spin-orbit coupling strength ξ. (b) Intrinsic anomalous Hall conductivity σ_{xy} at the Fermi energy in relation to the spin-orbit coupling strength ξ.*

The last step is to examine the temperature dependence of the intrinsic σ_{xy} by convoluting with the Fermi function in (5.84). The calculations are performed for the cases with the increased spin-orbit coupling strength $\xi = 2$, $\xi = 4$ and $\xi = 6$, while the temperature is set at $T = 150$K and at $T = 300$K. The results are shown in Fig.(6.11). The temperature dependence starts to become important near the Fermi energy at -0.1eV where σ_{xy} is a decreasing function. At the Fermi energy level, the value of σ_{xy} increases with T. Above the Fermi energy, the Fermi function vanishes and σ_{xy} becomes constant. As it is seen in Fig.(6.11), the effect of electronic temperature (up to room temperature) is rather small. The same is expected for the effect of magnetic fluctuations induced by temperature since the Curie temperature of bcc Fe is large (1043K).

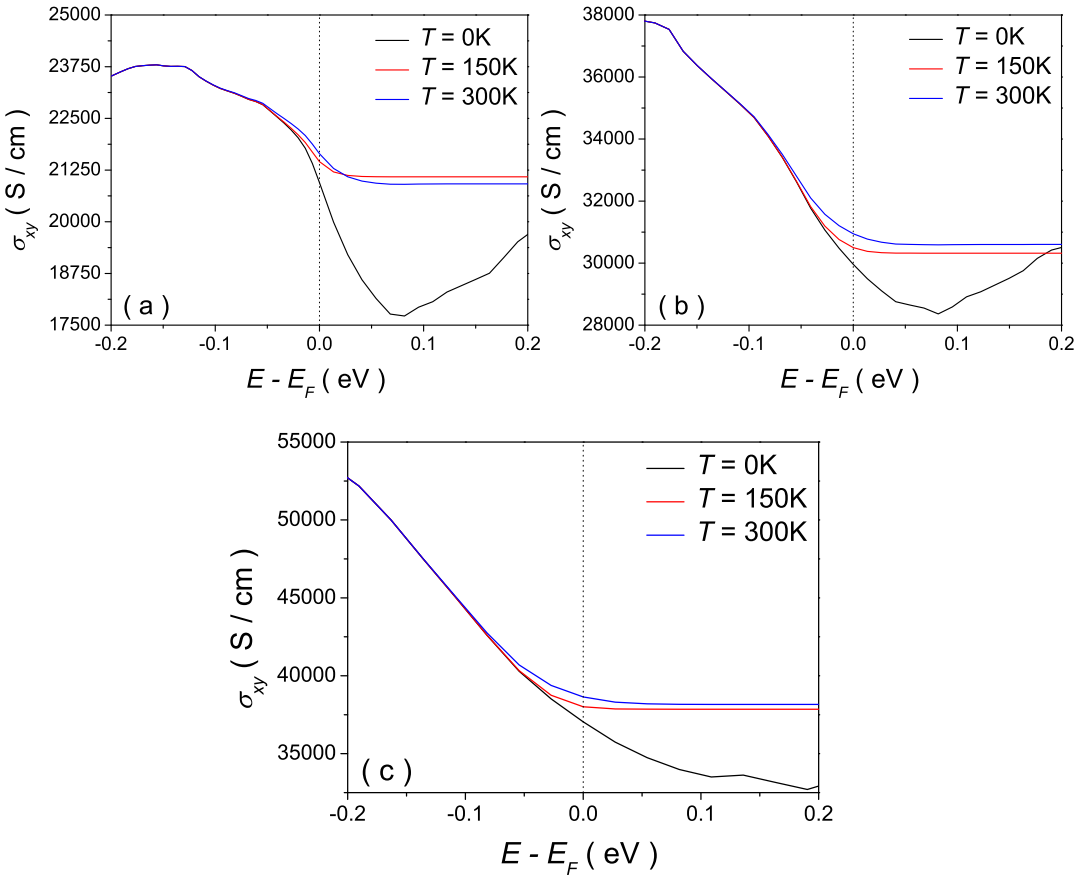

Figure 6.11: *Intrinsic anomalous Hall conductivity σ_{xy} in relation to temperature T, for different values of the spin-orbit coupling strength ξ. In (a) $\xi = 2$, in (b) $\xi = 4$ and in (c) $\xi = 6$. The results are presented relatively to the Fermi energy level.*

Chapter 7

Conclusion

In summary, a method was developed in order to calculate the Abelian Berry curvature within the framework of the full-potential scalar relativistic approximation to the Dirac equation, with the addition of a correction representing the spin-orbit coupling (SOC). This method was then used for the calculation of the intrinsic anomalous Hall conductivity (AHC). The studied system was the ferromagnetic bcc Fe.

At first, the Berry curvature was calculated over the Fermi surface. Its value was large only on "hot-spots" where avoided crossings of energy bands appear due to the SOC. These regions act as Berry curvature sources and, in order to be well depicted, a very dense **k**-points grid is needed. Then, after the decision of the suitable **k**-points grid, the energy resolved Berry curvature was calculated. Its spiky shape demanded a very fine energy partition. By progressively decreasing the energy partition, it was shown that it is unfeasible to reach convergence for the regular ($\xi = 1$) SOC strength. This difficulty was attributed to the nature of Fe as a material with weak SOC. As a result, smaller avoided crossings appear and the Berry curvature is larger at these regions. The convergence difficulty was overcome by artificially increasing the SOC strength to $\xi = 2$. That made possible to use a fine enough energy partition which would not cause numerical instabilities. As expected, the Berry curvature decreased because stronger SOC leads to larger splittings in the induced avoided crossings. The spiky character of the energy resolved Berry curvature was well depicted, while the peaks with the higher contributions were attributed to the d-electron states. Moreover, by further increasing the SOC strength to $\xi = 4$ and $\xi = 6$ the formed peaks became smoother and the overall shape of the energy resolved Berry curvature less spiky. An extrapolation from the converged values for $\xi = 6, 4,$ and 2 gives the result for $\xi = 1$.

Furthermore, the AHC was calculated from integrating the energy resolved Berry curvature over the energies. Although the behavior of AHC around the Fermi energy level was similar to other works, its value was calculated approximately 20 times larger. Additionally, the AHC increased non-linearly to the SOC strength as shown in previous works, with the results being again approximately 20 times larger. The origin of this

deviation was not found. Finally, the dependence of AHC on the electronic temperature was studied. It was found that, AHC increases together with the temperature, only in a small area of 0.1eV below the Fermi energy level. In general, the effect of the electronic temperature (up to room temperature) was rather small.

Appendix A

Berry curvature symmetries in k-space

The general symmetry properties of the Berry curvature in **k**-space is that, under time-reversal symmetry $\mathbf{\Omega}_n(-\mathbf{k}) = -\mathbf{\Omega}_n(\mathbf{k})$, while under space-inversion symmetry $\mathbf{\Omega}_n(-\mathbf{k}) = \mathbf{\Omega}_n(\mathbf{k})$ [6]. In systems where both time-reversal and space-inversion symmetries are present, the Berry curvature is identically zero. The ferromagnetic materials which are the subject of this thesis, exhibit only space-inversion symmetry because the spontaneous magnetization breaks the time-reversal symmetry. Apart from the above symmetries, the Berry curvature displays further constraints related to the elements of the space group of **k** [53].

The magnetic point group of a cubic metal with magnetization **M** along $[001]$, which is the case for bcc Fe studied in this thesis, is the $4/mm'm'$ [54]. It consists of 8 unitary and 8 anti-unitary elements, leading to a total of 16 elements. The elements of the unitary subgroup are $\{E, C_{2z}, C_{4z}, C_{4z-1}, I, S_{4z-1}, \sigma_z, S_{4z}\}$. The elements of the anti-unitary subgroup are $\{C_{2x}, C_{2y}, C_{2a}, C_{2b}, \sigma_x, \sigma_y, \sigma_{da}, \sigma_{db}\}$. In both subgroups, the last 4 elements are the inversion symmetric of the first 4. The Berry curvature behaves as an axial vector in **k**-space, that means that under a rotation R it changes as

$$\Omega'_n(R\mathbf{k}) = \det(R)\, R\, \Omega_n(\mathbf{k}), \tag{A.1}$$

in addition to the group velocity which behaves as a polar vector

$$\mathbf{v}'_n(R\mathbf{k}) = R\, \mathbf{v}_n(\mathbf{k}), \tag{A.2}$$

With that in mind and together with the relations for the Berry curvature tensor

$$\Omega^{\alpha}_n(\mathbf{k}) = \frac{1}{2}\epsilon_{\alpha\beta\gamma}\Omega_{n,\beta\gamma}(\mathbf{k}), \tag{A.3}$$

$$\Omega_{n,\beta\gamma}(\mathbf{k}) = -\Omega_{n,\beta\gamma}(\mathbf{k}), \tag{A.4}$$

$$\text{with} \quad (\alpha,\beta,\gamma) = (x,y,z), \quad \alpha \neq \beta \neq \gamma, \tag{A.5}$$

the constraints of the Berry curvature can be found in each case. The constraints from the first 4 symmetry elements can be seen in Table A.1 for the unitary elements and in Table A.2 for the anti-unitary elements. In these tables, also the behavior of the group velocity can be seen. For the rest inversion symmetric elements, the constraints can be found by the space-inversion symmetry property $\mathbf{\Omega}_n(-\mathbf{k}) = \mathbf{\Omega}_n(\mathbf{k})$. The essential point of the above discussion is that, only the z component $\Omega_z(\mathbf{k}) = \sum_n \Omega_n^z(\mathbf{k}) \neq 0$.

Unitary elements			
	$\mathbf{k}$	$\mathbf{v}_n(\mathbf{k})$	$\mathbf{\Omega_n}(\mathbf{k})$
E	(k_x, k_y, k_z)	(v_x, v_y, v_z)	$\Omega_n^x(k_x, k_y, k_z)$ $\Omega_n^y(k_x, k_y, k_z)$ $\Omega_n^z(k_x, k_y, k_z)$
C_{2z}	$(-k_x, -k_y, k_z)$	$(-v_x, -v_y, v_z)$	$\Omega_n^x(-k_x, -k_y, k_z) = -\Omega_n^x(k_x, k_y, k_z)$ $\Omega_n^y(-k_x, -k_y, k_z) = -\Omega_n^y(k_x, k_y, k_z)$ $\Omega_n^z(-k_x, -k_y, k_z) = \Omega_n^z(k_x, k_y, k_z)$
C_{4z}	$(-k_y, k_x, k_z)$	$(-v_y, v_x, v_z)$	$\Omega_n^x(-k_y, k_x, k_z) = -\Omega_n^y(k_x, k_y, k_z)$ $\Omega_n^y(-k_y, k_x, k_z) = \Omega_n^x(k_x, k_y, k_z)$ $\Omega_n^z(-k_y, k_x, k_z) = \Omega_n^z(k_x, k_y, k_z)$
C_{4z-1}	$(k_y, -k_x, k_z)$	$(v_y, -v_x, v_z)$	$\Omega_n^x(k_y, -k_x, k_z) = \Omega_n^y(k_x, k_y, k_z)$ $\Omega_n^y(k_y, -k_x, k_z) = -\Omega_n^x(k_x, k_y, k_z)$ $\Omega_n^z(k_y, -k_x, k_z) = \Omega_n^z(k_x, k_y, k_z)$

Table A.1: *Constraints on the Berry curvature and on the group velocity in* **k***-space for the first 4 unitary elements of the magnetic point group* $4/mm'm'$.

Anti-unitary elements			
	$\mathbf{k}$	$\mathbf{v}_n(\mathbf{k})$	$\boldsymbol{\Omega_n}(\mathbf{k})$
C_{2x}	$(k_x, -k_y, -k_z)$	$(v_x, -v_y, -v_z)$	$\Omega_n^x(k_x, -k_y, -k_z) = -\Omega_n^x(k_x, k_y, k_z)$ $\Omega_n^y(k_x, -k_y, -k_z) = \Omega_n^y(k_x, k_y, k_z)$ $\Omega_n^z(k_x, -k_y, -k_z) = \Omega_n^z(k_x, k_y, k_z)$
C_{2y}	$(-k_x, k_y, -k_z)$	$(-v_x, v_y, -v_z)$	$\Omega_n^x(-k_x, k_y, -k_z) = \Omega_n^x(k_x, k_y, k_z)$ $\Omega_n^y(-k_x, k_y, -k_z) = -\Omega_n^y(k_x, k_y, k_z)$ $\Omega_n^z(-k_x, k_y, -k_z) = \Omega_n^z(k_x, k_y, k_z)$
$C_{2\alpha}$	$(k_y, k_x, -k_z)$	$(v_y, v_x, -v_z)$	$\Omega_n^x(k_y, k_x, -k_z) = -\Omega_n^y(k_x, k_y, k_z)$ $\Omega_n^y(k_y, k_x, -k_z) = -\Omega_n^x(k_x, k_y, k_z)$ $\Omega_n^z(k_y, k_x, -k_z) = \Omega_n^z(k_x, k_y, k_z)$
$C_{2\beta}$	$(-k_y, -k_x, -k_z)$	$(-v_y, -v_x, -v_z)$	$\Omega_n^x(-k_y, -k_x, -k_z) = \Omega_n^y(k_x, k_y, k_z)$ $\Omega_n^y(-k_y, -k_x, -k_z) = \Omega_n^x(k_x, k_y, k_z)$ $\Omega_n^z(-k_y, -k_x, -k_z) = \Omega_n^z(k_x, k_y, k_z)$

Table A.2: *Constraints on the Berry curvature and on the group velocity in* **k***-space for the first 4 anti-unitary elements of the magnetic point group* $4/mm'm'$.

Bibliography

[1] M. V. Berry, "Quantal phase factors accompanying adiabatic changes", Proceedings of the Royal Society of London, Series A **392**, 45-57 (1984).

[2] D. Xiao, M.-C. Chang, and Q. Niu, "Berry phase effects on electronic properties", Reviews of Modern Physics, **82**, 1959-2007 (2010).

[3] M.-C. Chang and Q. Niu, "Berry phase, hyperorbits, and the Hofstadter spectrum: Semi-classical dynamics in magnetic Bloch bands", Physical Review B **53**, 7010-7023 (1996).

[4] M. Gradhand, D. V. Fedorov, F. Pientka, P. Zahn, I. Mertig, and B. L. Györffy, "Calculating the Berry curvature of Bloch electrons using the KKR method", Physical Review B **84**, 075113 (2011).

[5] D. Ködderitzsch, K. Chadova, and H. Ebert, "Linear response Kubo-Bastin formalism with application to the anomalous and spin Hall effects: A first-principles approach", Physical Review B **92**, 184415 (2015).

[6] Y. Mokrousov, "Berry phase in quantum mechanics", in 48th IFF Spring School 2017 " Topological Matter - Topological Insulators, Skyrmions and Majoranas", edited by S. Blügel, Y. Mokrousov, T. Schäpers, and Y. Ando, Vol. **139**, A6-A6.30 (Forschungszentrum Jülich GmbH, 2017).

[7] A. Bohm, A. Mostafazadeh, H. Koizumi, Q. Niu, and J. Zwanziger, *The Geometric Phase in Quantum Systems*, Springer-Verlag Berlin Heidelberg (2003).

[8] J. Zak, "Berry's phase for energy bands in solids", Physical Review Letters **62**, 2747-2750 (1989).

[9] J. Korringa, "On the calculation of the energy of a Bloch wave in a metal", Physica **13**, 392-400 (1947).

[10] W. Kohn and N. Rostoker, "Solution of the Schrödinger Equation in Periodic Lattices with an Application to Metallic Lithium", Physical Review B **94**, 1111-1120 (1954).

[11] T. H. Dupree, "Electron scattering in a crystal lattice", Annals of Physics, **15**, 63-78 (1961).

[12] J. L. Beeby, "The density of electrons in a perfect or imperfect lattice", Proceedings of the Royal Society of London, Series A **302**, 113-136 (1967).

[13] G. J. Morgan, "Bloch waves and scattering by impurities", Proceedings of the Physical Society **89**, 365-371 (1966).

[14] N. Papanikolaou, R. Zeller, and P. H. Dederichs, "Conceptual improvements of the KKR method", Journal of Physics: Condensed Matter **14**, 2799-2823 (2002).

[15] P. Mavropoulos and N. Papanikolaou, "The Korringa-Kohn-Rostoker (KKR) Green function method I. Electronic structure of periodic systems", *in Computational Nanoscience: Do It Yourself !*, edited by J. Grotendorst, S. Blügel, and D. Marx, NIC Series vol **31** (John von Neumann Institute for Computing, Forschungszentrum Jülich, 2006), pp. 131-158.

[16] S. Heers, "Effect of spin-orbit scattering on transport properties of low-dimensional dilute alloys", PhD thesis (RWTH Aachen, 2011).

[17] B. C. Zimmermann, "Ab initio description of transverse transport due to impurity scattering in transition-metals", PhD thesis (RWTH Aachen, 2014).

[18] G. Géranton, "Intrinsic and extrinsic spin-orbit torques from first principles", PhD thesis (RWTH Aachen, 2017).

[19] P. Rüßmann, "Spin scattering of topologically protected electrons at defects", PhD thesis (RWTH Aachen, 2018).

[20] A. Kosma, "Calculations of spin transport properties on topological insulator surfaces doped with magnetic defects", M.Sc. thesis, National and Kapodistrian University of Athens, 2018.

[21] N. Stefanou and R. Zeller, "Calculation of shape-truncation functions for Voronoi polyhedra", Journal of Physics: Condensed Matter **3**, 7599-7606 (1991).

[22] D. S. G. Bauer, "Development of a relativistic full-potential first-principles multiple scattering Green function method applied to complex magnetic textures of nano structures at surfaces", PhD thesis (RWTH Aachen, 2013).

[23] R. Zeller, "Multiple-scattering solution of Schrödinger's equation for potentials of general shape", Journal of Physics C: Solid State Physics **20**, 2347-2360 (1987).

[24] S. Blügel, H. Akai, R. Zeller, and P. H. Dederichs, "Hyperfine fields of $3d$ and $4d$ impurities in nickel", Physical Review B **35**, 3271-3283 (1987).

[25] S. Blügel, D. Bürgler, M. Morgenstern, C. M. Schneider, and R. Waser, "Spintronics - From GMR to Quantum Information: lecture notes of the 40th spring school 2009", Vol. **10** (Forschungszentrum Jülich GmbH, 2009).

[26] H. Weng, R. Yu, X. Hu, X. Dai, and Z. Fang, "Quantum anomalous Hall effect and related topological electronic states", Advances in Physics, **64**, 227-282 (2015).

[27] N. Nagaosa, J. Sinova, S. Onoda, A. H. MacDonald, and N. P. Ong, "Anomalous Hall effect", Review of Modern Physics **82**, 1539–1592 (2010).

[28] E. H. Hall, "On a New Action of the Magnet on Electric Currents", American Journal of Mathematics **2**, 287–292 (1879).

[29] E. H. Hall, "XVIII. On the Rotational Coefficient in nickel and cobalt", The London, Edinburgh, and Dublin Philosophical Magazine and Journal of Science **12**, 157–172 (1881).

[30] R. Karplus and J.M. Luttinger, "Hall Effect in Ferromagnetics", Physical Review **95**, 1154–1160 (1954).

[31] J. Smit, "The spontaneous hall effect in ferromagnetics I", Physica **21**, 877–887 (1955).

[32] J. Smit, "The spontaneous hall effect in ferromagnetics II", Physica **24**, 39–51 (1958).

[33] L. Berger, "Side-Jump Mechanism for the Hall Effect of Ferromagnets", Physical Review B **2**, 4559–4566 (1970).

[34] T. Jungwirth, Qian Niu, and A. H. MacDonald, "Anomalous Hall Effect in Ferromagnetic Semiconductors", Physical Review Letters **88**, 207208 (2002).

[35] Z. Fang, N. Nagaosa, K. S. Takahashi, A. Asamitsu, R. Mathieu, T. Ogasawara, H. Yamada, M. Kawasaki, Y. Tokura, and K. Terakura, "The Anomalous Hall Effect and Magnetic Monopoles in Momentum Space", Science **302**, 92-95 (2003).

[36] Y. Yao, L. Kleinman, A. H. MacDonald, J. Sinova, T. Jungwirth, D.-S. Wang, E. Wang, and Q. Niu, "First Principles Calculation of Anomalous Hall Conductivity in Ferromagnetic bcc Fe", Physical Review Letters **92**, 037204 (2004).

[37] X. Wang, J. R. Yates, I. Souza, and D. Vanderbilt, "*Ab initio* calculation of the anomalous Hall conductivity by Wannier interpolation", Physical Review B **74**, 195118 (2006).

[38] Y. Yao, Y. Liang, D. Xiao, Q. Niu, S.Q. Shen, X. Dai, and Z. Fang, "Theoretical evidence of the Berry-phase mechanism in anomalous Hall transport: First-principles studies of $CuCr_2Se_{4-x}Br_x$", Physical Review B **75**, 020401 (2007).

[39] F. D. M. Haldane, "Berry Curvature on the Fermi Surface: Anomalous Hall Effect as a Topological Fermi-Liquid Property", Physical Review Letters **93**, 206602 (2004).

[40] X. Wang, D. Vanderbilt, J. R. Yates, and I. Souza, "Fermi-surface calculation of the anomalous Hall conductivity", Physical Review B **76**, 195109 (2007).

[41] S. Onoda, N. Sugimoto, and N. Nagaosa, "Intrinsic Versus Extrinsic Anomalous Hall Effect in Ferromagnets", Physical Review Letters **97**, 126602 (2006).

[42] G. Sundaram and Q. Niu, "Wave-packet dynamics in slowly perturbed crystals: Gradient corrections and Berry-phase effects", Physical Review B **59**, 14915-14925 (1999).

[43] E. I. Blount, "Formalisms of Band Theory", in "*Solid State Physics*", edited by F.Seitz and D. Turnbull, Academic Press **13**, 305-373 (1962).

[44] P. Kramer and M. Saraceno, "*Geometry of the Time-Dependent Variational Principle in Quantum Mechanics*", Lecture Notes in Physics **140**, Springer-Verlag (1981).

[45] N. W. Ashcroft and N. D. Mermin, "*Solid State Physics*", Saunders College Publishing (1976).

[46] M. Gradhand, D. V. Fedorov, F. Pientka, P. Zahn, I. Mertig, and B. L. Györffy, "First-principle calculations of the Berry curvature of Bloch states for charge and spin transport of electrons", Journal of Physics: Condensed Matter **24**, 213202 (2012).

[47] G. Y. Guo, Y. Yao, and Q. Niu, "*Ab initio* Calculation of the Intrinsic Spin Hall Effect in Semiconductors", Physical Review Letters **94**, 226601 (2005).

[48] Y. Yao and Z. Fang, "Sign Changes of Intrinsic Spin Hall Effect in Semiconductors and Simple Metals: First-Principles Calculations", Physical Review Letters **95**, 156601 (2005).

[49] Z. Slepian, "On Decoupling the Integrals of Cosmological Perturbation Theory", arXiv:1812.02728, preprint (2018).

[50] http://jukkr.fz-juelich.de.

[51] J. Weischenberg, F. Freimuth, S. Blügel, and Y. Mokrousov, "Scattering-independent anomalous Nernst effect in ferromagnets", Physical Review B **87**, 060406 (2013).

[52] P. N. Dheer, "Galvanomagnetic Effects in Iron Whiskers", Physical Review **156**, 637-644 (1967).

[53] M.-T. Suzuki, T. Koretsune, M. Ochi, and R. Arita, "Cluster multipole theory for anomalous Hall effect in antiferromagnets", Physical Review B **95**, 094406 (2017).

[54] A. P. Cracknell, "Time-Reversal Degeneracies in the Band Structure of a Ferromagnetic Metal", Physical Review B **1**, 1261-1263 (1970).